On the Formation and the Isomer Specific Detection of Methylacetylene (CH_3CCH), Propene (CH_3CHCH_2), Cyclopropane (c-C_3H_6), Vinylacetylene (CH_2CHCCH), and 1,3-Butadiene ($CH_2CHCHCH_2$) from Interstellar Methane Ice Analogues

Journal:	*Physical Chemistry Chemical Physics*
Manuscript ID	CP-ART-06-2018-003921.R2
Article Type:	Paper
Date Submitted by the Author:	28-Aug-2018
Complete List of Authors:	Abplanalp, Matthew; University of Hawaii, Gobi, Sandor; University of Hawaii, Department of Chemistry Kaiser, Ralf I; University of Hawaii,

On the Formation and the Isomer Specific Detection of Methylacetylene (CH_3CCH), Propene (CH_3CHCH_2), Cyclopropane (c-C_3H_6), Vinylacetylene (CH_2CHCCH), and 1,3-Butadiene ($CH_2CHCHCH_2$) from Interstellar Methane Ice Analogues

Matthew J. Abplanalp[1,2], Sándor Góbi[1,2,3], Ralf I. Kaiser[1,2,*]

[1]W. M. Keck Research Laboratory in Astrochemistry, University of Hawaii at Manoa, Honolulu, HI, 96822, USA

[2]Department of Chemistry, University of Hawaii at Manoa, Honolulu, HI, 96822, USA

[3]Current Address: CQC, Department of Chemistry, University of Coimbra, 3000-535, Coimbra, Portugal

ABSTRACT

Pure methane (CH_4) ices processed by energetic electrons under ultra-high vacuum conditions to simulate secondary electrons formed via galactic cosmic rays (GCRs) penetrating interstellar ice mantles have been shown to produce an array of complex hydrocarbons with the general formulae: C_nH_{2n+2} (n = 4–8), C_nH_{2n} (n = 3–9), C_nH_{2n-2} (n = 3–9), C_nH_{2n-4} (n = 4–9), and C_nH_{2n-6} (n = 6–7). By monitoring the *in situ* chemical evolution of the ice combined with temperature programmed desorption studies (TPD) and tunable single photon ionization coupled to a reflectron time-of-flight mass spectrometer, specific isomers of C_3H_4, C_3H_6, C_4H_4, and C_4H_6 were probed. These isomer specific experiments confirmed the synthesis of methylacetylene (CH_3CCH), propene (CH_3CHCH_2), cyclopropane (c-C_3H_6), vinylacetylene (CH_2CHCCH), 1-butyne ($HCCC_2H_5$), 2-butyne (CH_3CCCH_3), 1,2-butadiene ($H_2CCCH(CH_3)$), and 1,3-butadiene ($CH_2CHCHCH_2$) with yields of $2.17 \pm 0.95 \times 10^{-4}$, $3.7 \pm 1.5 \times 10^{-3}$, $1.23 \pm 0.77 \times 10^{-4}$, $1.28 \pm 0.65 \times 10^{-4}$, $4.01 \pm 1.98 \times 10^{-5}$, $1.97 \pm 0.98 \times 10^{-4}$, $1.90 \pm 0.84 \times 10^{-5}$, and $1.41 \pm 0.72 \times 10^{-4}$ molecules eV^{-1}, respectively. Mechanistic studies exploring the formation routes of methylacetylene, propene, and vinylacetylene were also conducted. Several of the above isomers, methylacetylene, propene, vinylacetylene, and 1,3-butadiene, have repeatedly been shown to be important precursors in the formation of polycyclic aromatic hydrocarbons (PAHs), but until now their interstellar synthesis has remained elusive.

1. Introduction

During the last decades, methylacetylene (CH_3CCH), propene (CH_3CHCH_2), vinylacetylene (CH_2CHCCH), and 1,3-butadiene ($CH_2CHCHCH_2$) have received considerable attention from the astrochemistry and astronomy communities due to their critical roles in astrochemical processes.[1, 2] Interestingly, each of these molecules have been shown to be capable of forming precursors to polycyclic aromatic hydrocarbons (PAHs), prototype PAHs, and PAHs themselves.[3] Specifically, methylacetylene emerged as a precursor in the formation of PAHs such as indene (C_9H_8) as well as 5- and 6-methyl-1H-indene ($C_{10}H_{10}$) through the bimolecular reaction with a phenyl radical (C_6H_5) and via a reaction with the para-tolyl radical ($C_6H_4CH_3$), respectively.[4-7] Methylacetylene has also been used in models to explain Titan's atmospheric chemistry.[8-11] Similarly, propene (CH_3CHCH_2) produced resonantly stabilized free radicals (RSFRs) – precursors to PAHs – in gas-phase reactions with carbon atoms (C) and dicarbon molecules (C_2) forming the methylpropargyl radical (C_4H_5) as well as 1- and 3-vinylpropargyl radical (C_5H_5), respectively.[12-14] Also, vinylacetylene (CH_2CHCCH) has been suggested as a hydrocarbon important for Titan's chemistry,[11, 15, 16] and forms prototype PAHs such as naphthalene ($C_{10}H_8$), 1- and 2-methylnaphthalene ($C_{11}H_{10}$), and ortho-benzyne (o-C_6H_4) in the gas phase.[17-20] Finally, 1,3-butadiene ($CH_2CHCHCH_2$) is also fundamental as an essential building block in gas-phase growth of prototypical PAHs through reactions with dicarbon (C_2) to form the phenyl radical (C_6H_5), with the tolyl radical ($C_6H_4CH_3$) forming 6-methyl-1,4-dihydronaphthalene ($C_{11}H_{12}$), and with the ethynyl radical (CCH) producing benzene (C_6H_6).[21-23]

The C_3H_4 isomer methylacetylene (CH_3CCH) was first observed towards Sagittarius B2 and Orion A via the $5_0 \rightarrow 4_0$ transitions at 85 GHz.[24, 25] Subsequently, methylacetylene has been detected in several astronomical surveys toward TMC-1, SgrB2, PKS 1830-211, L1544, NGC 7538 IRS9, tentatively in NCG 4418, and recently for the first time in a photo-dissociation region via the Horsehead nebula at fractional abundances – in all sources – of a few 10^{-9} with respect to molecular hydrogen.[26-33] This results in a column density of about 8×10^{13} molecules cm^{-2}.[34] Besides the interstellar medium (ISM), the methylacetylene molecule has also been observed in our Solar System on Jupiter, Saturn, Uranus, and Titan.[35-38] Many years later the C_3H_6 isomer propene (CH_3CHCH_2) was detected in the ISM using 13 rotational lines from 84 to 104 GHz toward TMC-1 and more recently in the cold cores Lupus-1A, L1495B, L1521F, and

Serpens South 1a with fractional abundances of a few 10^{-9}.[34, 39] This calculates to a column density of about 4×10^{13} molecules cm^{-2}.[34] Propene has also been detected in the atmosphere of Titan.[40] However, none of the other C3 hydrocarbons, allene (CH_2CCH_2), cyclopropene (c-C_3H_4), or cyclopropane (c-C_3H_6), has been detected in the ISM. Although the C4 hydrocarbons vinylacetylene ($H_2CCHCCH$) and 1,3–butadiene ($H_2CCHCHCH_2$) have remained elusive in the ISM they are still astrophysically important molecules. Vinylacetylene has been shown to react with the phenyl radical and produce the PAH naphthalene[1, 18] and has been suggested to be an important hydrocarbon for Titan's chemistry.[11, 15, 16] Similarly, 1,3–butadiene can react with the ethynyl radical (CCH) to form benzene (C_6H_6),[23] with the phenyl radical (C_6H_5) to form 1,4-dihydronaphthalene ($C_{10}H_{10}$),[41] or with the tolyl radical (C_7H_7) to form 5- and 6-methyl-1,4-dihydronaphthalene ($C_{11}H_{12}$).[42]

Recently, it was shown that the methylacetylene molecule cannot be synthesized via gas-phase reactions alone.[27, 43] An extensive review of the chemical pathways leading to methylacetylene in the gas phase concluded that there are no efficient gas-phase synthetic pathways available to reproduce the observed abundances of this molecule in the cold ISM.[27] Here, the main gas-phase source of methylacetylene was proposed to be through ion-molecule reactions that produce $C_3H_5^+$ followed by dissociative recombination reactions with minor formation pathways via neutral-neutral reactions. Since gas-phase reactions were not able to reproduce the ISM abundance of methylacetylene, surface reactions taking place on interstellar grains have been investigated. These gas-phase species were assumed to stick to the cold dust grains and then undergo hydrogenation at the ultra-cold ISM temperatures of 10 K. The methylacetylene molecule was shown to form via the hydrogenation of C_3 which could then be further hydrogenated to propene. However, the model including gas-phase and grain-surface reactions cannot reproduce the observed methylacetylene abundance by more than an order of magnitude. These failed attempts to reproduce the methylacetylene abundance show that important formation pathways are still missing at low temperatures.[27, 28, 33]

It has also been proposed that the propene molecule was synthesized via gas-phase reactions. However, a comprehensive analysis of these hypothesized reactions shows that some have considerable entrance barriers, which makes them inefficient in the cold ISM.[27, 44] Following the failure to reproduce the observations of propene in the ISM with pure gas-phase mechanisms

surface reactions on low temperature ISM grains were considered as an alternate pathway once again. Similar to methylacetylene, models incorporating solely surface reactions producing propene – from the hydrogenation of methylacetylene – fail to reproduce the observed abundance by an order of magnitude.[27] Another pathway investigated the recombination of radicals, from exploding ice mantles, in a high-density gas-phase model, but this again failed to replicate the observed abundances.[45-47] Although these models show a better agreement than pure gas-phase models to the observed abundance there is clearly a significant production route lacking at ISM temperatures.[27, 34]

Although, vinylacetylene and 1,3-butadiene have remained undetected in the ISM, several reactions have shown that they can be produced under ISM conditions. Vinylacetylene has been shown to be a product of several gas-phase reactions such as the ethynyl radical reacting with ethylene (C_2H_4),[11, 48, 49] the ethynyl radical with propene,[48] and the methylidyne radical (CH) with propene.[50] Vinylacetylene has also been a proposed product in several theoretical gas-phase studies, some modeling of Titan's atmosphere, from ethynyl radical reacting with ethylene (C_2H_4), propene (C_3H_6), and 1-butene (C_4H_8).[51, 52] The formation of vinylacetylene via solid-phase pathways have also been proposed such as in acetylene (C_2H_2) ices via the recombination of a vinyl radical (C_2H_3) and ethynyl radical,[53] or possibly through the recombination of excited acetylene molecules.[54] Utilizing some of these reaction pathways vinylacetylene has been incorporated into ISM chemical models.[55-57] Also, 1,3-butadiene can be formed in gas-phase reactions such as propene reacting with the methylidyne radical,[23, 50, 58, 59] as well as the reaction of the methylidyne radical with *trans*-butene.[50] This important molecule has also been speculated to form in ices through the recombination of two vinyl radicals.[23] Although multiple studies have been carried out on the production pathways of these four molecules – methylacetylene, propene, vinylacetylene, 1,3-butadiene – their formation pathways remain mostly speculative and with the lack of agreement of models, using these reactions, with observation shows that they are ill-defined and clearly there are missing synthetic routes producing these astrochemically important molecules.

Here, we demonstrate that methylacetylene, propene, vinylacetylene, and 1,3-butadiene can be formed in pure methane ice when exposed to ionizing radiation in the form of energetic electrons which mimic secondary electrons produced from the passage of galactic cosmic rays

(GCRs) through ISM ices.[60-63] Although no pure methane ice has been detected in space it is an ice constituent at levels up to 11 % with respect to water in the ISM[64] and as a major constituent on Pluto via the recent New Horizons mission.[65, 66] The current study utilizes single photon ionization coupled with a reflectron time-of-flight mass spectrometer (PI-ReTOF-MS) to detect methylacetylene, propene, vinylacetylene, and the 1,3-butadiene isomers selectively. Traditionally, Fourier-transform infrared spectroscopy (FTIR) and electron impact quadrupole mass spectrometry (EI-QMS) have been used to identify molecules formed in ISM analog ices that have been exposed to ionizing radiation. However, FTIR can only firmly identify individual molecules that are very small, such as carbon monoxide (CO), water (H_2O), carbon dioxide (CO_2), and methane (CH_4), all of which have been detected as constituent of ISM ices, or functional groups of more complex molecules.[64] As molecules become more complex their infrared vibrations begin to overlap and make definitive identification based solely on FTIR analysis impossible. Figure 1 shows an overlay of mid-IR spectra for the hydrocarbons methane (CH_4), ethylene (C_2H_4), ethane (C_2H_6), allene (CH_2CCH_2), methylacetylene (CH_3CCH), propane (C_3H_8), and butane (C_4H_{10}), which clearly shows that the hydrocarbons larger than C2 begin to have extensive overlap of their most intense vibrations making their identification very difficult. Gas-phase analysis of the subliming molecules from the irradiated ice can provide complementary assignments to FTIR analysis. Typically this is accomplished with EI-QMS, but this technique often utilizes an ionization energy of 70 eV which not only ionizes most organic molecules but also causes their extensive fragmentation. Figure 2 shows an overlay of the fragmentation pattern of the hydrocarbons methane (CH_4), ethylene (C_2H_4), ethane (C_2H_6), allene (CH_2CCH_2), methylacetylene (CH_3CCH), propane (C_3H_8), and butane (C_4H_{10}). Here, several of the molecules' molecular ions are not the most intense signal corresponding to the parent molecule and many of the fragments of these hydrocarbons have overlapping masses. In order to provide a more sensitive analysis of the processed ice, these limited capabilities of FTIR and EI-QMS have been further complemented by incorporating single photon ionization coupled with a reflectron time-of-flight mass spectrometer (PI-ReTOF-MS), which allows isomer specific analysis of the subliming products from the ISM analog ices.[67-76] This technique utilizes soft photon ionization which results in minimal or no fragmentation of the parent molecule.[68, 69, 77] Further, the tunable photoionization energy allows for specific isomers to be identified based upon each isomer's ionization energy.[78-83]

2. Experimental

All experiments were completed in an ultrahigh vacuum (UHV) chamber at pressures of typically 3×10^{-11} torr.[68, 84, 85] A UHV compatible closed-cycle helium compressor (Sumitomo Heavy Industries, RDK-415E) connected to a cold finger, constructed of oxygen free high conductivity copper, is interfaced to the UHV chamber using a differentially pumped rotary feedthrough (Thermionics Vacuum Products, RNN-600/FA/MCO) and a UHV compatible bellow (McAllister, BLT106) that allows it to be rotated in the horizontal plane and/or translated in the vertical plane, respectively. The substrate, a highly reflective silver mirror, is interfaced to the cold finger via indium foil to ensure thermal conductivity. Also, a glass capillary array is used to deposit the gases onto the silver target. Typical background pressures of 5×10^{-8} Torr in the UHV chamber over a few minutes resulted in the desired thickness of methane (Specialty Gases of America, 99.999%) ice to be deposited.[86] During this deposition the ice thickness was determined by monitoring on line and *in situ* the interference pattern produced during the gas deposition via a HeNe laser (λ = 632.8 nm; CVI Melles-Griot; 25-LHP-230) reflecting off of the silver substrate into a photodiode.[87-89] The ice thickness was determined to be 590 ± 50 nm from this method by using a refractive index n = 1.280 ± 0.008.[90] Using a modified Lambert-Beer relationship with absorption coefficients of 3.95×10^{-19}, 1.40×10^{-17}, 1.29×10^{-20}, 3.89×10^{-19}, 8.15×10^{-19}, and 8.76×10^{-20} cm molecule^{-1} and integrated areas for the respective infrared bands 2814 ($\nu_2 + \nu_4$), 3010 (ν_3), 4114 ($\nu_2 + 2\nu_4$), 4202 ($\nu_1 + \nu_4$), 4301 ($\nu_3 + \nu_4$), and 4528 ($\nu_2 + \nu_3$) yielded an average thickness of 440 ± 130 nm, which is in agreement with the more accurate laser interferometry method.[90]

Once the ice was deposited a Fourier-transform infrared spectrometer (FTIR; Nicolet 6700), which probes the active infrared vibrational modes of the reactant and product molecules within the sample, was utilized to continuously analyze the ice on line and *in situ* before, during, and after processing. The FTIR was operated in absorption-reflection-absorption mode at a reflection angle of 45º to the substrate normal in the mid-IR region from 5000 to 500 cm^{-1} with a resolution of 4 cm^{-1} at 2 minute intervals, which allowed for 30 spectra to be collected during the one hour of irradiation with 5 keV electrons.[91-94] Following the irradiation phase the ice was held isothermal at 5 K for one hour. Next, the substrate was heated to 300 K through a controlled ramp rate of 0.5 K min^{-1} (temperature programmed desorption; TPD). The electron gun (Specs EQ 22-35) is positioned 100 cm from the sample, and the energetic electrons processed 1.0 ± 0.1

cm^2 of the methane ice striking it at an incidence angle of 70° relative to the surface normal of the substrate for 1 hour with a current of 30 nA, which results in a fluence of $(6.7 \pm 0.5) \times 10^{14}$ electrons cm^{-2}.[95, 96] Utilizing Monte Carlo simulations via CASINO 2.42 software[97] the mean average penetration depth of the energetic electrons was calculated to be 410 ± 20 nm and only up to 5 % of the energy absorbed by the ice occurs beyond 250 nm. Using a density of 0.47 g cm^{-3} for methane it was determined that the average energy deposited into the ice was 3.5 ± 1.1 eV $molecule^{-1}$ of methane (Table S1).[98-100] It was calculated that ices inside cold dense clouds in the ISM receive an energy dose of 0.3–3 eV $molecule^{-1}$ over 10^6 –10^7 years from GCRs, which is the energetic processing that is attempted to be replicated in the present manuscript. Furthermore, although the low flux of interstellar like photons and GCRs can be achieved no experimental laboratory can exactly mimic ISM irradiation conditions due to the length of the residence times of the ices (>10^6 years), and therefore the total dose absorbed by the ice is a reasonable way to compare the processing of ices across experimental labs and to the ISM.[101] Also, as seen from average penetration depth of the electrons, chemical reactions take place throughout the bulk of the ice which has traditionally been considered inert and not considered in astrochemical models.[79]

During the TPD phase, the subliming molecules were monitored via a QMS (Extrel, Model 5221) and PI-ReTOF-MS. Here, the QMS instrument monitors a mass range from 1-300 amu with a 70 eV electron impact ionization source and an emission current of 2 mA by operating in residual gas analyzer (RGA) mode.[102-104] In order to monitor the subliming molecules with PI-ReTOF-MS the substrate was rotated 180° to face the ReTOF and cannot be monitored by FTIR at the same time, thus requiring multiple experiments for each system. The PI-ReTOF-MS technique consists of ionizing subliming molecules via single photon ionization in the form of pulsed coherent VUV light.[105-107] The generation of the VUV light used was accomplished via four-wave difference mixing, which requires the interaction of three photons in a non-linear medium to produce a fourth VUV photon. Here, the photons generated from a Nd:YAG (Spectra-Physics, PRO-270-30 or PRO-250-30) were used directly to produce VUV at an energy of 10.49 eV (118 nm), via non-resonant four-wave mixing, or acted as a pump laser for a separate dye laser. Two dye lasers were used that has the capability of tuning from 350-630 nm (Sirah, Cobra-Stretch) or 400-900 nm (Sirah, Precision Scan), and either dye laser output can be frequency doubled, or the former dye laser output can be frequency tripled with BBO crystals.

The laser outputs, from the Nd:YAG and/or dye lasers are then focused into a pulse valve housing emitting the non-linear medium, which was either krypton or xenon in the present experiments. After the interaction region containing the non-linear medium a lithium fluoride (LiF) lens is used to separate the input wavelengths from the desired VUV wavelength utilizing the difference in refractive index across wavelengths for LiF. The VUV light was then directed in front of the substrate to ionize subliming molecules, which were then detected with the ReTOF. Finally, the intensity was then measured with a NIST calibrated photodiode, which is typically optimized for each VUV energy to around 10^{12} photons s^{-1}. To distinguish which C_3H_4, C_3H_6, C_4H_4, and C_4H_6 isomers were formed in the processed methane ice four different photoionization energies of 10.49 eV (λ= 118.2 nm), 9.77 eV (λ= 126.9 nm), 9.45 eV (λ= 131.2 nm), and 9.15 eV (λ= 135.5 nm) were employed (Fig. 3). Next, once a molecule was ionized it was detected utilizing a reflectron time-of-flight mass spectrometer (Jordan TOF products, Inc.). Here, the ions were detected via a dual chevron configured multichannel plate (MCP). The MCP signal was then amplified with a fast pre-amplifier (Ortec 9305) followed by shaping via a 100 MHz discriminator. A personal-computer-based multichannel scaler (FAST ComTec, P7888-1 E) then recorded the spectra using 4 ns bin widths triggered at 30 Hz (Quantum Composers, 9518), with 3600 sweeps in a mass spectrum which corresponds to a 1 K change in temperature of the substrate per mass spectrum.

3. Results

3.1 Infrared Spectroscopy

A complete analysis utilizing FTIR of the electron irradiated methane ice has been previously discussed.[100] Briefly, six products propane (C_3H_8), ethane (C_2H_6), ethyl radical (C_2H_5), ethylene (C_2H_4), acetylene (C_2H_2), and the methyl radical (CH_3) were detected via several infrared absorptions.[108, 109] Kinetic fitting of the temporal profiles via the numerical solution of a system of coupled differential equations allowed the extraction of a reaction mechanism producing the small molecules observed in the infrared and was extrapolated to explain the more complex species observed via PI-ReTOF-MS.[100] However, Figure 4 shows infrared stretches that can be assigned to several small hydrocarbons propane (C_3H_8, ν_s, 2961 cm^{-1}), ethane (C_2H_6, ν_5, 2883 cm^{-1}), ethylene (C_2H_4, ν_9, 3093 cm^{-1}), acetylene (C_2H_2, ν_3, 3266 cm^{-1}), and methane (CH_4, ν_3, 3008 cm^{-1}) and yet several of these infrared stretches remain well past the known sublimation

temperature of their assignments, showing that they have contributions to their signal from other more complex species with higher sublimation temperatures. By comparing literature values or depositing pure samples of methylacetylene, propene, vinylacetylene, and 1,3-butadiene and recording their infrared spectrum it is clear that several of these infrared stretches belong to these molecules (ESI; Fig. S1; Table S2 and S3). Furthermore, by monitoring these infrared stretches during TPD several can be correlated with sublimation events of methylacetylene via its ν_6 fundamental at 2959 cm^{-1} and propene by the ν_3 (2970 cm^{-1}), ν_{15} (2940 cm^{-1}), ν_4 (2915 cm^{-1}), and $2\nu_7$ (2883 cm^{-1}) infrared peaks (Fig. S2). However, many more complex hydrocarbons were also able to be detected with PI-ReTOF-MS.

3.2 PI-ReTOF-MS

During TPD the subliming molecules were monitored via PI-ReTOF-MS (PI = 10.49 eV; 118 nm), which detected products belonging to five hydrocarbon groups with the generic formulae: C_nH_{2n+2} (n = 4-8), C_nH_{2n} (n = 3-9), C_nH_{2n-2} (n = 3-9), C_nH_{2n-4} (n = 4-9), and C_nH_{2n-6} (n = 6-7) (Fig. 5). Interestingly, ions corresponding to the molecular formulae C_3H_4, C_3H_6, C_4H_4, and C_4H_6 were all detected in this experiment which could correspond to the astrophysically important molecules methylacetylene (*m/z* = 40), propene (*m/z* = 42), vinylacetylene (*m/z* = 52), and 1,3-butadiene (*m/z* = 54), respectively (Fig. 6). Each of the above molecular formulae have multiple isomers associated with them and therefore the contribution due to each isomer to the overall signal is unknown. Therefore, several experiments utilizing tunable photoionization were needed to further discriminate which specific isomers were formed from the electron irradiated methane ice (ESI; Table S4).

3.2.1 C_3H_4

The ion signal detected at *m/z* = 40 can only correspond to the molecular formula C_3H_4, which has three possible isomers: methylacetylene (CH_3CCH; IE = 10.36 ± 0.01 eV), allene (CH_2CCH_2; PI = 9.69 ± 0.01 eV), and cyclopropene (c-C_3H_4; IE = 9.67 ± 0.01 eV) (Fig. 6a).[110] The ion signal began to be detected at about 75 K, peaked at 87 K, and continued to sublime until 110 K where it then returned to the baseline. To better determine the identity of these signals calibration experiments were also performed (ESI). Here, a mixture containing 1% methylacetylene, 1% propene, and 1% 1,3-butadiene in methane was deposited and then monitored during TPD with PI-ReTOF-MS (PI = 10.49 eV) (Fig. S3). This calibration

experiment detected a similar peak at *m/z* = 40 subliming from 75-110 K. Despite the very close match of the unknown ion signal to the known methylacetylene signal it could still be due to any of the three isomers, but most likely had some contribution from the methylacetylene isomer. In order to definitively identify the isomers contributing to the signal the PI energy was tuned to 9.77 eV (Fig. 6e). Interestingly, no signal was detected at *m/z* = 40 at this PI energy, and therefore it is only due to the methylacetylene isomer and neither of the other two isomers. As expected no ion signal was detected at PI energies of 9.45 eV or 9.15 eV either. Further, by accounting for the photoionization cross section at 10.49 eV of 18.9 Mb and utilizing the PI-ReTOF-MS correction factor derived from the calibration ices the yield of methylacetylene was calculated to be $2.17 \pm 0.95 \times 10^{-4}$ molecules eV^{-1} (Table 1 and S4).

3.2.2 C_3H_6

The signal detected at *m/z* = 42 is due to a hydrocarbon of the molecular formula C_3H_6, which can only be due to cyclopropane (c-C_3H_6; IE = 9.86 ± 0.04) or propene (CH_3CHCH_2; IE = 9.73 ± 0.01).[110] Here, the signal ranged from 68-91 K and peaked at 77 K (Fig. 6b). The calibration experiment signal of propene showed a similar onset sublimation temperature of 67 K (Fig. S3). Although the onset sublimation temperature of propene matches nicely with the unknown *m/z* = 42 signal it could also be due to cyclopropane as either isomer can be ionized at a PI of 10.49 eV. Switching to a PI energy of 9.77 eV, signal is still detectable at *m/z* = 42, which can only be due to propene (Fig. 6f). This detection unambiguously identifies propene as a contributor to the ion signal. However, further investigation of the ion signals – after accounting for differences in flux of the experiments and the photoionization cross section of the isomers (Table S4) – detected with PI energies of 10.49 eV and 9.77 eV reveals that a small portion of the 10.49 eV signal, where both isomers are able to be ionized, from about 80-90 K was due to the cyclopropane isomer (Fig. 6f inset). As expected no ion signal was detected at PI energies of 9.45 eV or 9.15 eV because neither of these isomers will be photoionized. After, applying the experimentally derived correction factor from the calibration ices to the photoionization cross section corrected data the yields of propene and cyclopropane were calculated to be $3.7 \pm 1.5 \times 10^{-3}$ molecules eV^{-1} and $1.23 \pm 0.77 \times 10^{-4}$ molecules eV^{-1}, respectively (Table 1). This shows a much larger production of propene and corresponds to a 30 ± 22 : 1 ± 0.75 ratio of propene to cyclopropane.

3.2.3 C_4H_4

Signal was also detected at *m/z* = 52, which corresponds to the molecular formula C_4H_4 and could be due to vinylacetylene (CH_2CHCCH; IE = 9.58 ± 0.02), 1,2,3-butatriene (CH_2CCCH_2; IE = 9.16 ± 0.02), cyclobutadiene (c-C_4H_4; IE = 8.16 ± 0.03), and/or methylenecyclopropene (CH_2(c-C_3H_2); IE = 8.15 ± 0.03) (Fig. 6c).[110] The sublimation profile of *m/z* = 52 extended from 94-120 K. Tuning the PI energy to 9.77 eV revealed no change of the ion signal, within the error bars, after correcting for differences in photon flux and isomer cross sections (Fig. 6g). This result is expected as all of the above isomers are able to be photoionized at both 10.49 eV and 9.77 eV. However, adjusting the PI energy to 9.45 eV resulted in no signal detection at *m/z* = 52 and therefore the only C_4H_4 isomer produced in the methane ice can be unmistakably assigned to vinylacetylene (Fig. 6g). Also, there was no signal detected at PI = 9.15 eV. Following the previously described procedure the yield of vinylacetylene produced from the irradiated methane ice was calculated to be $1.90 \pm 0.84 \times 10^{-5}$ molecules eV^{-1} (Table 1).

3.2.4 C_4H_6

PI-ReTOF-MS also detected an ion signal at *m/z* = 54 belonging to the molecular formula C_4H_6, which may be due to any of the four different isomers: 1,3-butadiene ($H_2CCHCHCH_2$; IE = 9.07 eV), 1,2-butadiene ($H_2CCCH(CH_3)$; IE = 9.03 eV), 1-butyne ($HCCC_2H_5$; IE = 10.18 eV), and/or 2-butyne (CH_3CCCH_3; IE = 9.58 eV) (Fig. 6d).[110] The ion signal was observed to sublime from 85-115 K with multiple peak events, which may be due to several different isomers subliming at different temperatures. However, the previously described calibration sublimation profile of 1,3-butadiene, subliming from 87-115 K, matched very nicely to the unknown ion signal suggesting that the signal is at least partially due to this isomer (Fig. S3). To discriminate which isomers contributed to *m/z* = 54 the PI energy was changed to 9.77 eV, 9.45 eV, and 9.15 eV to no longer ionize certain isomers (Fig. 3). At all of the PI energies *m/z* = 54 was detected, showing that there could be contributions from multiple isomers (Fig. 6d). However, the detection of *m/z* = 54 at 9.15 eV unambiguously identifies 1,3-butadiene as a product. After correcting the ion signal, for flux differences and each isomer's photoionization cross sections at each PI, the amount that each isomer contributed to the total signal at 10.49 eV could be calculated (Table S4). First, the signal detected at 9.15 eV can only belong to 1,3-butadiene, and because the signal can be corrected to the amount that it contributed to the signal at 9.45 eV it can be subtracted from the total signal detected for *m/z* = 54 at 9.45 eV. The remaining signal can

then only be due to 1,2-butadiene. This procedure was repeated for the signal at 9.77 eV by subtracting the corrected 1,3-butadiene and 1,2-butadiene signals to determine the contribution due to 2-butyne. This procedure was repeated as well for the 10.49 eV ion signal by subtracting the influences from 1,3-butadiene, 1,2-butadiene, and 2-butyne to determine the amount of 1-butyne produced (Fig. 6h). The yields for 1,3-butadiene, 1,2-butadiene, 2-butyne, and 1-butyne were determined to be $1.41 \pm 0.72 \times 10^{-4}$ molecules eV^{-1}, $1.97 \pm 0.98 \times 10^{-4}$ molecules eV^{-1}, $4.01 \pm 1.98 \times 10^{-5}$ molecules eV^{-1}, and $1.28 \pm 0.65 \times 10^{-4}$ molecules eV^{-1}, respectively, which corresponds to a ratio of $3.5 \pm 2.5 : 4.9 \pm 3.4 : 1 \pm 0.7 : 3.2 \pm 2.3$ (Table 1).

4. Discussion

4.1 Reaction Mechanism & Energetics

In order to deduce the mechanistic details about the synthesis of methylacetylene, propene, and vinylacetylene a retro-synthesis of each molecule was performed to understand the different pathways, and ultimately what starting compounds to use (Fig. 7). The complexity of the 1,3-butadiene formation pathways is beyond the scope of the current manuscript. The energetics of these pathways are investigated to help explain why certain mechanisms are viable while others remain inaccessible (Table 2). Furthermore, these mechanisms may provide insight into the relative ratios determined above.

4.1.1 C_3H_4

Methylacetylene could be formed via three possible pathways: insertion of a carbene radical (CH_2) into an acetylene carbon–hydrogen bond, recombination of a methyl radical (CH_3) with an ethynyl radical (CCH), and addition of a methyl radical (CH_3) to acetylene forming the allyl radical (CH_3CHCH) followed by hydrogen loss producing methylacetylene (Fig. 7a). In order to determine the methylacetylene reaction mechanism mixed ices of D4-methane (CD_4) and acetylene (C_2H_2), with a ratio of 1:1, were irradiated to unravel which pathways produced methylacetylene in methane ices (Fig. 7a).[111, 112] Here, the detection of *m/z* = 42 ($C_3H_2D_2$) shows that methylacetylene was produced via insertion of the carbene radical. Alternatively, the detection of *m/z* = 43 (C_3HD_3) would prove that the radical recombination of the methyl radical with the ethynyl radical occurs to produce methylacetylene. It should be noted that the third pathway, via methyl radical addition to acetylene, results in an identical mass-to-charge ratio as

the radical recombination route and therefore these two pathways are indecipherable no matter what isotopic substitution scheme is used.

Figure 8 shows both *m/z* = 42 and 43 were detected subliming from the D4-methane–acetylene ice at a photoionization energy of 10.49 eV. These ion signals could belong to any of the deuterium substituted C_3H_4 isotopomers (*m/z* = 42 and 43) or possibly from C_3H_6 isomers (*m/z* = 42). To determine which molecules were formed, several tunable experiments were carried out. Utilizing a PI energy of 9.93 eV will photoionize all C_3H_4 isotopomers *except* methylacetylene (CH_3CCH; IE = 10.36 ± 0.01 eV) and all C_3H_6 isomers. Therefore, any change in *m/z* = 42 or 43 can be correlated with methylacetylene. Here, we see that *m/z* = 43 drops to the baseline and thus the only molecule responsible for the *m/z* = 43 signal is methylacetylene (Fig. 8b). Similarly, Figure 8a displays the change in *m/z* = 42 at 9.93 eV (red line) from 10.49 eV (black dashed-line), and the difference of these two signals can only correspond to methylacetylene (orange line). Here, the methylacetylene (orange line) is the difference spectrum produced by subtracting the 9.93 eV signal from the 10.49 eV signal. Furthermore, because the signal at *m/z* = 43 at 10.49 eV was solely due to methylacetylene this peak was scaled and subtracted from *m/z* = 42 at 10.49 eV, and an overlay of this difference spectrum with the *m/z* = 42 ion signal recorded at PI = 9.93 eV match very well confirming the assignment of methylacetylene (Fig. S4a).

However, there are still other ions adding to the signal *m/z* = 42 at 10.49 eV (black dashed-line). By changing the PI energy to 9.77 eV we can further constrain what molecules are responsible for this signal as any change from 9.93 eV to 9.77 eV will be due to the contribution of cyclopropane (c-C_3H_6; IE = 9.86 ± 0.04 eV). At PI = 9.77 eV (blue line) another change in the *m/z* = 42 TPD profile is observed confirming the presence of cyclopropane, but a signal is still present (Fig. 8a). To determine the cyclopropane contribution (cyan line) the signal recorded for *m/z* = 42 at 9.77 eV (blue line) was subtracted from the signal recorded at 9.93 eV (red line). The remaining signal at 9.77 eV (blue line) could be due to the C_3H_4 isotopomers allene (D_2CCCH_2; IE = 9.69 ± 0.01 eV), or cyclopropene (c-$C_3H_2D_2$; IE = 9.67 ± 0.01 eV), and/or the C_3H_6 isomer propene (CH_3CHCH_2; IE = 9.73 ± 0.01 eV). However, by irradiating a pure acetylene ice an identical signal at *m/z* = 42 was detected, which can only be due to C_3H_6 isomers, and is most likely the propene isomer due to its match with the 9.77 eV peak at *m/z* = 42 from the D4-

methane–acetylene ice experiment (Fig. S4b). Using this information it was possible to determine what portion of the 9.93 eV spectrum was due to cyclopropane (Fig. 8a).

Now that the viable reaction pathways have been detected the reactions' energetics to produce methylacetylene can be discussed (Table 2). The formation of the methyl radical (reaction (1)) and carbene radical (reaction (2)) are endoergic by 4.44 eV (429 kJ mol^{-1}) and 5.13 eV (495 kJ mol^{-1}), respectively, which can be accounted for by the impinging electrons (Table S1). Also, the formation of the ethynyl radical is endoergic and requires 5.73 eV (553 kJ mol^{-1}; reaction (3)) to form. The radical recombination pathway for the formation of methylacetylene via the recombination of the methyl and ethynyl radicals has no barrier and is exoergic by -5.42 eV (-523 kJ mol^{-1}; reaction (4)). Alternatively, the insertion of the carbene radical into the acetylene molecule is also barrierless, when in the singlet excited state (a^1A_1), and exoergic by -4.82 eV (-465 kJ mol^{-1}; reaction (5)). However, the final pathway of methyl radical addition to the acetylene molecule (reaction (6)) has a barrier of 0.34 eV (33 kJ mol^{-1}) and is endoergic by 0.31 eV (30 kJ mol^{-1}).[113, 114] The energetics of these pathways show that both the radical recombination (reaction (4)) and insertion (reaction (5)) pathways are feasible as they are barrierless and exoergic, but that the addition route (reaction (6)) is unlikely at the low temperature of the experiment (5 K) under thermal equilibrium as it has a barrier and is also an endoergic reaction. Here, the detection of m/z = 42 and 43 with the methylacetylene portion in a ratio of 1.0 ± 0.2 : 2.0 ± 0.4, respectively, shows that the radical recombination pathway to methylacetylene is preferred (reaction (4)). This preference matches with the energetics as the formation of the methyl radical and recombination of it with the ethynyl radical are less endoergic and more exoergic, respectively, when compared to the carbene formation and its insertion into the acetylene molecule. In summary, methylacetylene is formed via radical recombination and carbene insertion in a ratio of 2.0 ± 0.4 : 1.0 ± 0.2.

4.1.2 C_3H_6

Similarly, propene is able to be formed through three routes: insertion of a carbene radical (CH_2) into an ethylene carbon–hydrogen bond, recombination of a methyl radical (CH_3) with a vinyl radical (C_2H_3), and addition of a methyl radical (CH_3) to ethylene forming the propyl radical ($CH_3CH_2CH_2$) followed by hydrogen loss forming propene. Propene's reaction mechanism was probed via mixed ices of methane and D4-ethylene in a ratio of 1:1 (Fig. 7b).

Detection of *m/z* = 45 from this experiment shows that propene is produced via radical recombination of the methyl radical with the vinyl radical. Alternatively, the detection of *m/z* = 46 means that propene was produced from the insertion of the carbene radical into an ethylene carbon-hydrogen bond. Again, it should be noted that the third pathway, via methyl radical addition using the vinyl radical, results in an identical mass-to-charge ratio as the radical recombination route. The results of these experiments are shown in Figure 9, and confirmed the presence of both *m/z* = 45 and 46 at a photoionization energy of 10.49 eV. Here, the only ions that can be associated with *m/z* = 45 and 46 are the propene and cyclopropane isotopomers. By tuning the photoionization energy to 9.77 eV only propene (IE = 9.73 ± 0.01 eV) will be ionized and not the cyclopropane (IE = 9.86 ± 0.04 eV) isotopomer. The results of this tunable experiment confirm the formation of propene via both the radical recombination pathway as well as the insertion route as an ion signal was detected at both *m/z* = 45 and 46. Here, radical recombination formed solely the propene isotopomer (Fig. 9a). However, after accounting for the flux and photoionization cross section of propene at PI = 9.77 eV the *m/z* = 46 TPD profile had a portion of its signal that could not be accounted for by only propene. Therefore, a portion of the *m/z* = 46 signal at 10.49 eV must belong to cyclopropane (Fig. 9b).

As stated above for methylacetylene, the formation of the methyl radical and carbene radical are endoergic by 4.44 eV (429 kJ mol^{-1}) and 5.13 eV (495 kJ mol^{-1}), respectively (reactions (1) and (2)). Also, the formation of the vinyl radical is endoergic and requires 4.71 eV (454 kJ mol^{-1}; reaction (7)) to form. The insertion of the carbene radical into the ethylene molecule is barrierless, if the carbene is in the singlet excited state (a^1A_1), and exoergic by -4.72 eV (-455 kJ mol^{-1}; reaction (8)). The recombination of the methyl and ethynyl radicals also has no barrier though and is exoergic by -4.29 eV (-414 kJ mol^{-1}; reaction (9)). Finally, the addition of the methyl radical to ethylene leading to propene and a hydrogen atom (reaction (10)) has a barrier of 1.92 eV (185 kJ mol^{-1}) and is endoergic by 0.41 eV (40 kJ mol^{-1}).[113, 114] Again, the addition reaction mechanism involving a barrier is not likely under thermal conditions due to the low temperature of the system. The detection of propene via *m/z* = 45 and 46 in a ratio of 1.5 ± 0.4 : 1 ± 0.25, at 9.77 eV, shows that radical recombination is preferred for propene synthesis (reaction (9)). This is again reflected by the energetics as reactions (8) and (9) have very similar exoergicities. However, it is possible that the carbene radical needed to form propene is also used to form cyclopropane and therefore the competing pathway results in a lower yield of propene

via carbene insertion. In summary, propene is formed from both radical recombination and carbene insertion with a ratio of 1.5 ± 0.4 : 1 ± 0.25.

4.1.3 C_4H_4

Next, the vinylacetylene molecule's formation route was investigated taking into consideration the following pathways: addition of dicarbon (C_2) to ethylene (reaction (12)), or recombination of an ethynyl radical (C_2H) with a vinyl radical (C_2H_3, reaction (13)). The reaction mechanism was probed via mixed ices of D2-acetylene and $^{13}C_2$-ethylene, with a ratio of 1:1 (Fig. 7c). Detection of *m/z* = 54 would confirm that vinylacetylene was synthesized from the addition of dicarbon to ethylene, and the detection of *m/z* = 55 from this experiment reveals that vinylacetylene is produced via radical recombination of the ethynyl radical with the vinyl radical.

Figure 10 shows that both *m/z* = 54 and 55 were detected at a PI energy of 10.49 eV, but several tunable experiments were also needed to decipher which C_4H_4 isomers this signal might be due to. Since, vinylacetylene has an IE of 9.58 ± 0.02 eV any photoionization energy below this will no longer ionize this molecule, but all other C_4H_4 species if they were produced. The detection of a signal for *m/z* = 54 (PI = 9.45 eV) shows that it is not solely due to vinylacetylene, but with no signal detected at PI = 8.41 eV it was confirmed to be only due to 1,2,3-butatriene and vinylacetylene (Fig. 10a). Next, the non-detection of *m/z* = 55 at PI = 9.45 eV shows that the radical recombination pathway can only synthesize the vinylacetylene isotopomer (Fig 10b).

Again, the reactions to form the vinyl radical and ethynyl radical are endoergic and require 4.71 eV (454 kJ mol^{-1}; reaction (7)) and 5.73 eV (553 kJ mol^{-1}; reaction (3)), respectively. The ethynyl radical can lose another hydrogen atom forming dicarbon and this process is also endoergic by 4.90 eV ((473 kJ mol^{-1}; reaction (11)). The dicarbon molecule, which is closed shell, has been shown to add barrierlessly to the ethylene molecule's double bond initially forming a reaction intermediate, which is then followed by isomerization to eventually form 1,2,3-butatriene or vinylacetylene, which agrees with the detection of both isomers.[115] The pathway forming vinylacetylene is exoergic by -6.09 eV (-588 kJ mol^{-1}; reaction (12)).

Alternatively the recombination of the vinyl and ethynyl radicals to form vinylacetylene is also barrierless and exoergic by -5.90 eV (569 kJ mol^{-1}; reaction (13)). Finally, the addition

reaction of vinyl radical with acetylene has been shown to have a barrier of 0.06 eV (6.2 kJ mol^{-1}) and is exoergic by -0.17 eV (-16 kJ mol^{-1}, reaction (14)).[52] Meanwhile, the ethynyl radical addition to ethylene does not have a barrier and is exoergic by -1.19 eV (-115 kJ mol^{-1}, reaction (15)).[52] Here, the detection of *m/z* = 54 and 55 in a ratio of 1 ± 0.3 : 11 ± 3 shows that radical recombination is strongly preferred for vinylacetylene synthesis (reaction (13)). Previous gas-phase experiments have shown that the reaction of dicarbon with ethylene preferentially formed 1,2,3-butatriene, which can then isomerize to vinylacetylene and may explain what is observed in the present experiment.[115] This agrees with the current results with the preferential formation of vinylacetylene in that the radical recombination pathway is heavily favored over insertion. In summary, vinylacetylene is synthesized through radical recombination and the dicarbon addition with a ratio of 11 ± 3 : 1 ± 0.3.

5. Conclusions

Multiple studies have been conducted over the past decades to understand the astrochemical processes utilizing the C1 hydrocarbon methane (CH_4) and the C2 hydrocarbons ethane (C_2H_6), ethylene (C_2H_4), and acetylene (C_2H_2). Although a thorough analysis of the different pathways to small hydrocarbons available through these C1 and C2 precursors has been attempted, an isomer specific study of the complex hydrocarbons that are formed, deep within these ices from interaction with GCRs, was lacking until now. All of the hydrocarbon isomers detected here belong to a group in astrochemistry called complex organic molecules (COMs) – molecules having 6 or more atoms of carbon, hydrogen, nitrogen, and/or oxygen – which have been a key point of focus in recent years of laboratory astrophysics.[2] These COMs have been shown to be easily produced within the ice and not only through surface reactions.[79] The isomer specific identification of methylacetylene (CH_3CCH), propene (CH_3CHCH_2), cyclopropane (c-C_3H_6), vinylacetylene (CH_2CHCCH), 1-butyne ($HCCC_2H_5$), 2-butyne (CH_3CCCH_3), 1,2-butadiene ($H_2CCCH(CH_3)$), and 1,3-butadiene ($CH_2CHCHCH_2$) provides insight into the complex hydrocarbon chemistry taking place in the ISM. Specifically, the investigation of gas-phase PAH formation has been a heavily studied area as PAHs are suggested to exist in large abundances in the ISM and account for much of the cosmic carbon,[116-126] and may have biological precursor relevance when nitrogen substituted.[4,127, 128] Although some of the reaction pathways have been

elucidated, several of the precursors' formation pathways needed for these reactions have remained elusive until now (1. Introduction).

For the C3 hydrocarbons detected here methylacetylene has been repeatedly shown to be a key precursor in PAH formation through bimolecular reactions with the phenyl radical (C_6H_5), in the gas phase, to produce indene – a bicyclic aromatic hydrocarbon.[1, 4-7] Furthermore, the indene molecule has been shown to produce even more complex PAHs as large as chrysene ($C_{18}H_{12}$).[129] Also, pure methylacetylene has been shown to react with oxygen atoms to produce the complex oxygen containing molecules such as C_3H_4O and $C_3H_4O_2$, which consist of several interesting isomers including some which have already been detected in the ISM.[130] It should be noted that allene (CH_2CCH_2), a second C_3H_4 isomer that is nearly isoenergetic to methylacetylene, was not detected here, but is also very important for the formation of PAHs such as indene, 5-methyl-1H-indene, and 6-methyl-1H-indene.[1, 5, 7, 119] While methylacetylene was the only isomer produced in the solid phase from methane ices bimolecular reactions under single collisions have determined that the reaction of the methylidyne radical (CH; $X^2\Pi$) with ethylene forms only the allene isomer.[131] Therefore, the methylacetylene and allene isomers can be used to trace if the chemical evolution of different ISM environments have contributions from solid- or gas-phase chemistry, respectively. Additionally, the propene isomer has also been shown to produce RSFRs which can then yield PAHs, and also react with the phenyl radical producing indene (C_9H_8).[1, 12-14] Propene was also recently shown to be a precursor in the formation of propylene oxide (c-C_3H_6O), which was the first chiral molecule detected in the ISM.[132-134] Also, the cyclopropane molecule, the only other possible C_3H_6 isomer of propene, detected in these experiments represents the simplest cycloalkane. While cyclopropane is not a PAH precursor, it does prove that the complex hydrocarbons produced from solid methane ice can be cyclic.

Furthermore, the C4 hydrocarbon isomers selectively observed in the present manuscript have also been shown to produce PAHs. Vinylacetylene can react with the phenyl radical producing the prototypical PAH known as naphthalene ($C_{10}H_8$),[18, 135] as well as with the para-tolyl radical ($C_6H_4CH_3$) forming 2-methylnaphthalene ($C_{11}H_{10}$),[19] and finally with the meta-tolyl radical ($C_6H_4CH_3$) creating 1-methylnaphthalene ($C_{11}H_{10}$).[20] Similarly, 1,3-butadiene forms multiple PAH precursors as well as PAH molecules. Intriguingly, the reaction of 1,3-butadiene with the ethynyl radical produces benzene, and the injection of 1,3-butadiene from dust grains greatly

improves model abundances of benzene again showing a link between the solid and gas phase.[23] Meanwhile, 1,3-butadiene's reaction with the phenyl radical generates 1,4-dihydronaphthalene ($C_{10}H_{10}$),[41, 136] the reaction with the tolyl radical forms 5- and 6-methyl-1,4-dihydronaphthalene ($C_{11}H_{12}$),[42] and its reaction with the 1-napthyl radical synthesizes dihydrophenanthrene ($C_{14}H_{12}$).[137] Furthermore, 1,3-butadiene can also react with the cyano radical to form pyridine (C_9H_5N),[3, 138] and its reaction with pyridyl radicals (C_5H_4N) can produce 1,4-dihydro (iso)quinolone (C_9H_9N).[3] The other C_4H_6 isomers detected here, 1,2-butadiene, 1-butyne, and 2-butyne, have also been shown to react with dicarbon to make RSFRs.[139]

The present manuscript shows that the coupling of traditional astrochemistry techniques with new highly sensitive analytical techniques can elucidate the complex hydrocarbon chemistry available in simple ISM ices. Figure 11 depicts a global reaction scheme for the chemistry stemming from a methane ice. The formation routes of propane, ethane, ethylene, and acetylene, from methane ices have been experimentally determined.[140] Now, the C3 hydrocarbons are complete with the addition of the C_3H_4 and C_3H_6 reaction pathways. Finally, the C4 hydrocarbons have been expanded upon as well with the addition of C_4H_4 formation pathways. Furthermore, by studying the effects of adding other constituents to the ice, most importantly water, will help unravel the chemical complexity of hydrocarbon containing ISM ices, and the current manuscripts provides the necessary first step in understanding these more realistic and complex mixtures. Finally, the results from this manuscript show a direct link between the solid phase, beyond surface reactions, and gas-phase chemistry taking place in the ISM. The inclusion of these solid-phase chemical reactions occurring within the ice rather than only on the surface has greatly enhanced the agreement of astrochemical models with observations for several COMs detected in the ISM.[79]

Conflicts of interest

There are no conflicts to declare.

Acknowledgements

RIK and MJA thank the US National Science Foundation (AST-1505502) for support to conduct the experiments and data analysis. The experimental apparatus was financed by the W. M. Keck Foundation through an equipment grant.

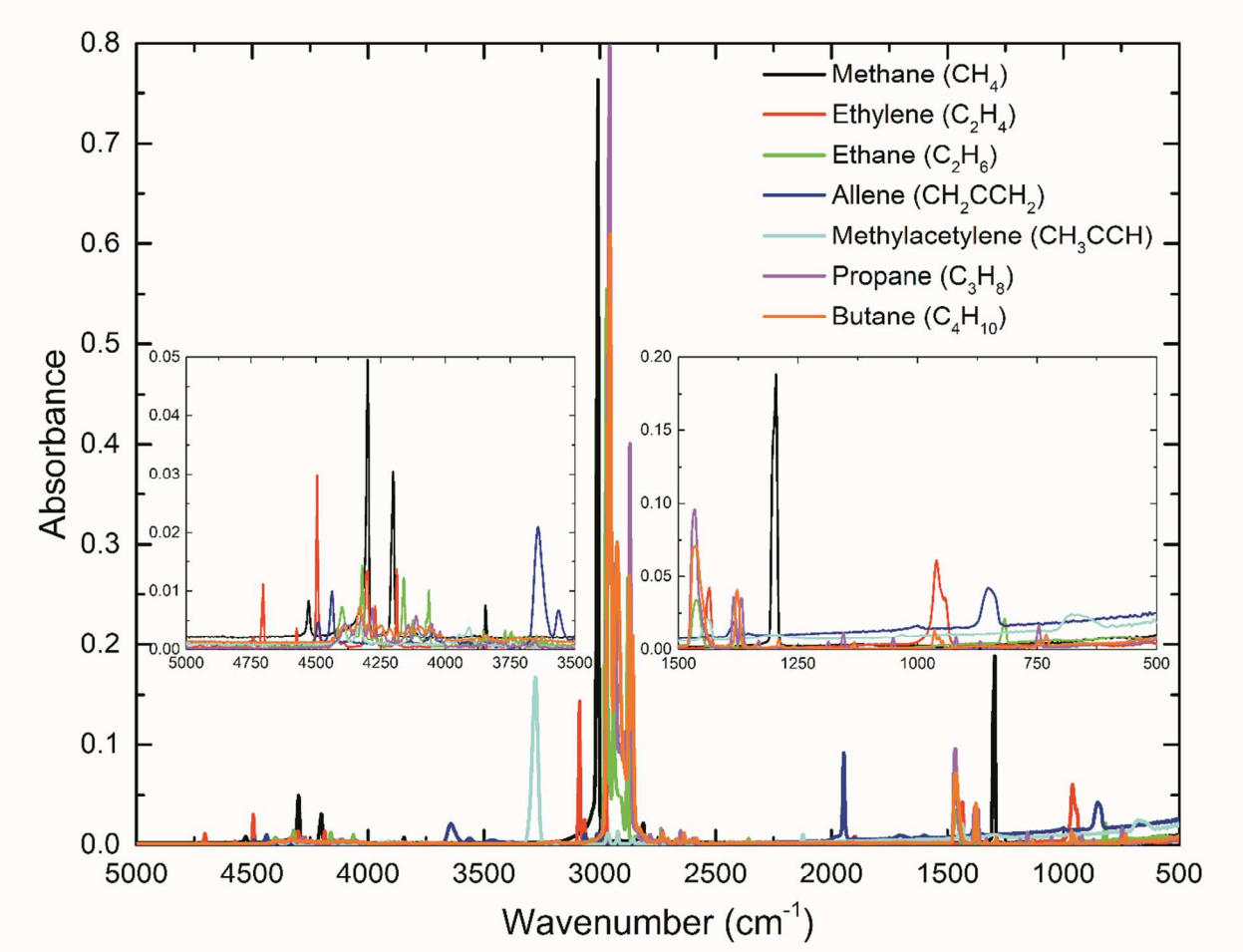

Fig. 1 Infrared spectra from 5000-500 cm^{-1} of several pure unprocessed ices at 5 K. The left inset is a 16× magnification of 5000-3500 cm^{-1} and the right inset is a 4× magnification of 2000-500 cm^{-1}.

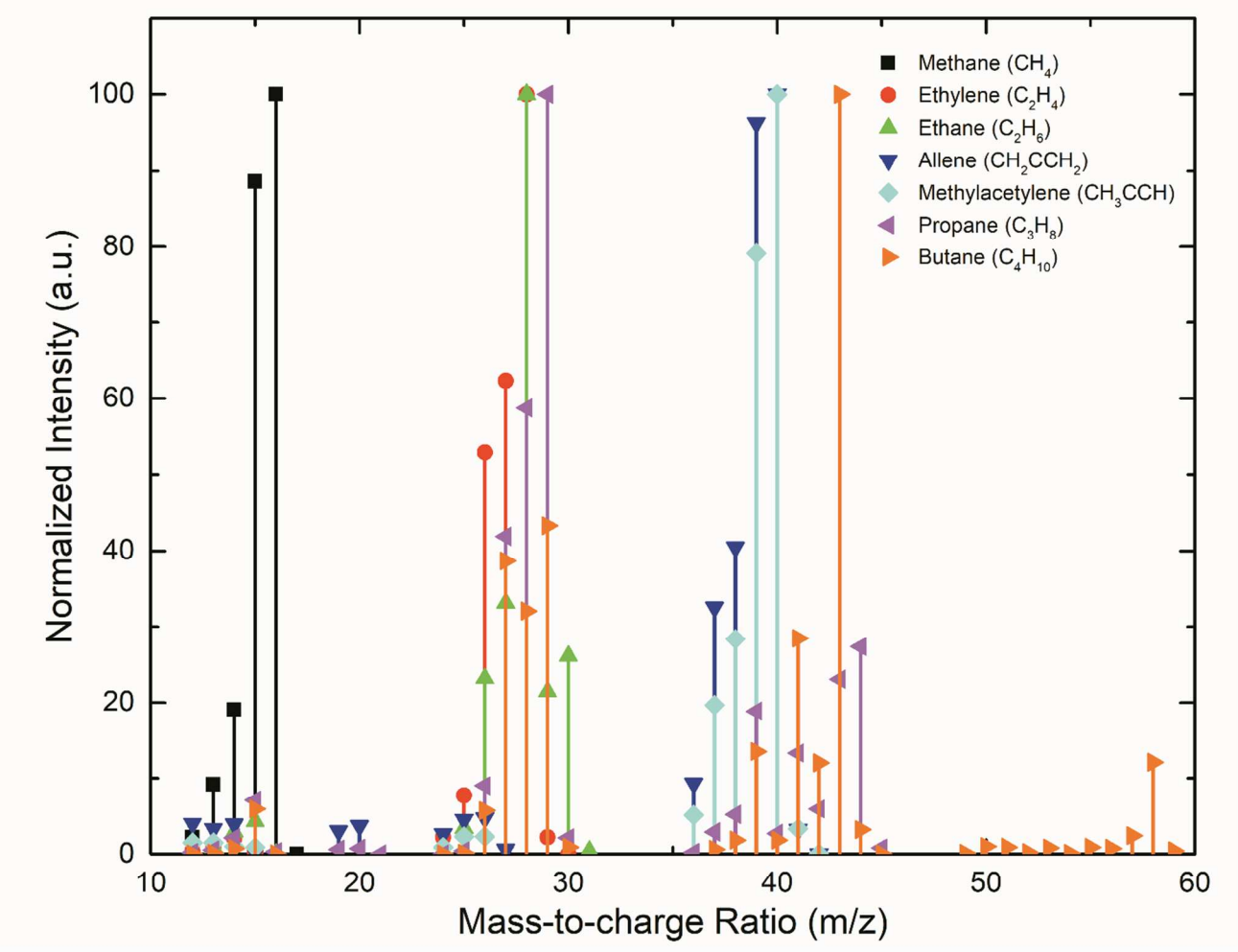

Fig. 2 Overlay of electron ionization, at 70 eV, fragmentation patterns of several hydrocarbons (https://webbook.nist.gov/chemistry/).

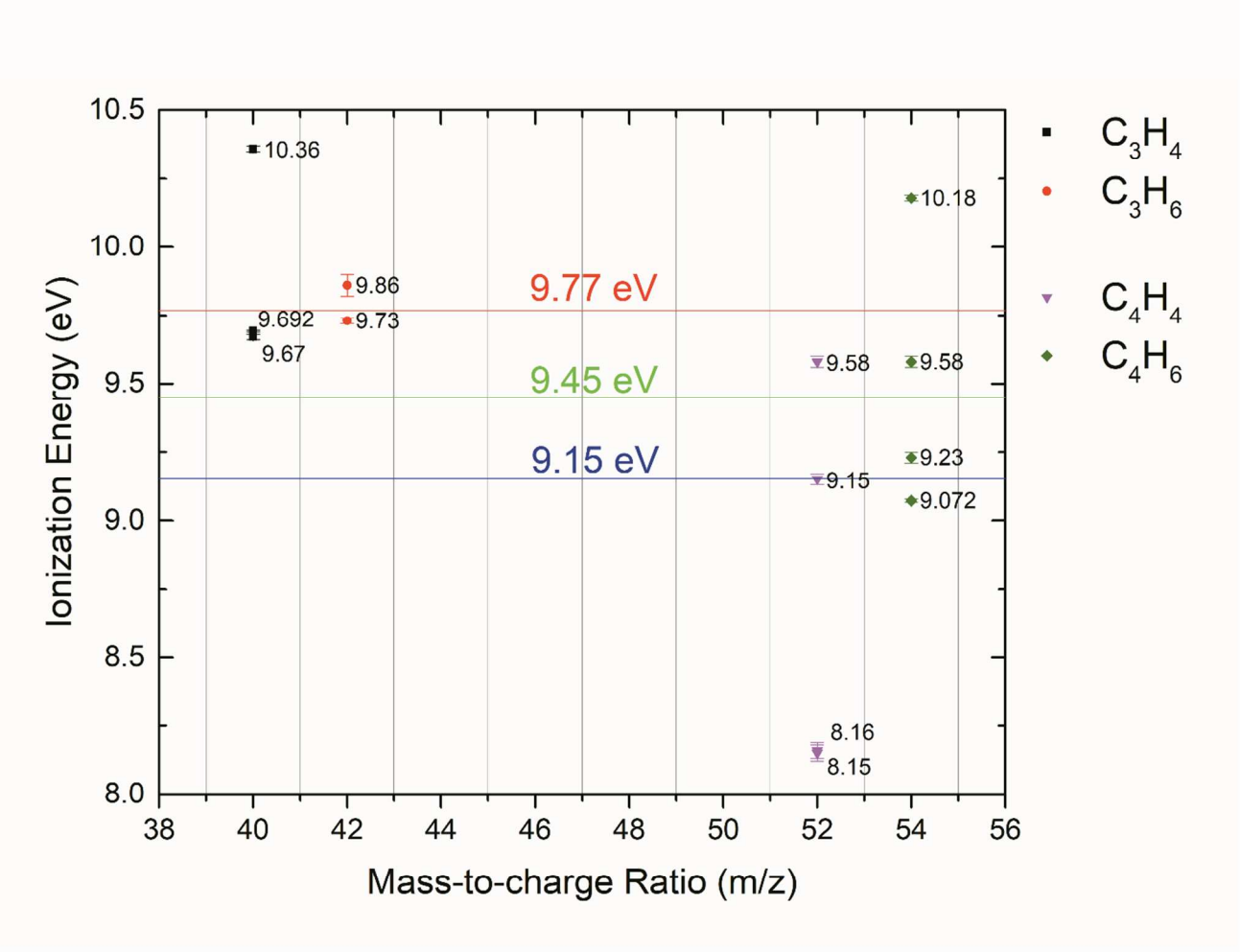

Fig. 3 Scheme for PI energy to discriminate the C_3H_4 isomers (black squares), C_3H_6 isomers (red circles), C_4H_4 isomers (pink triangles), and C_4H_6 isomers (green diamonds).

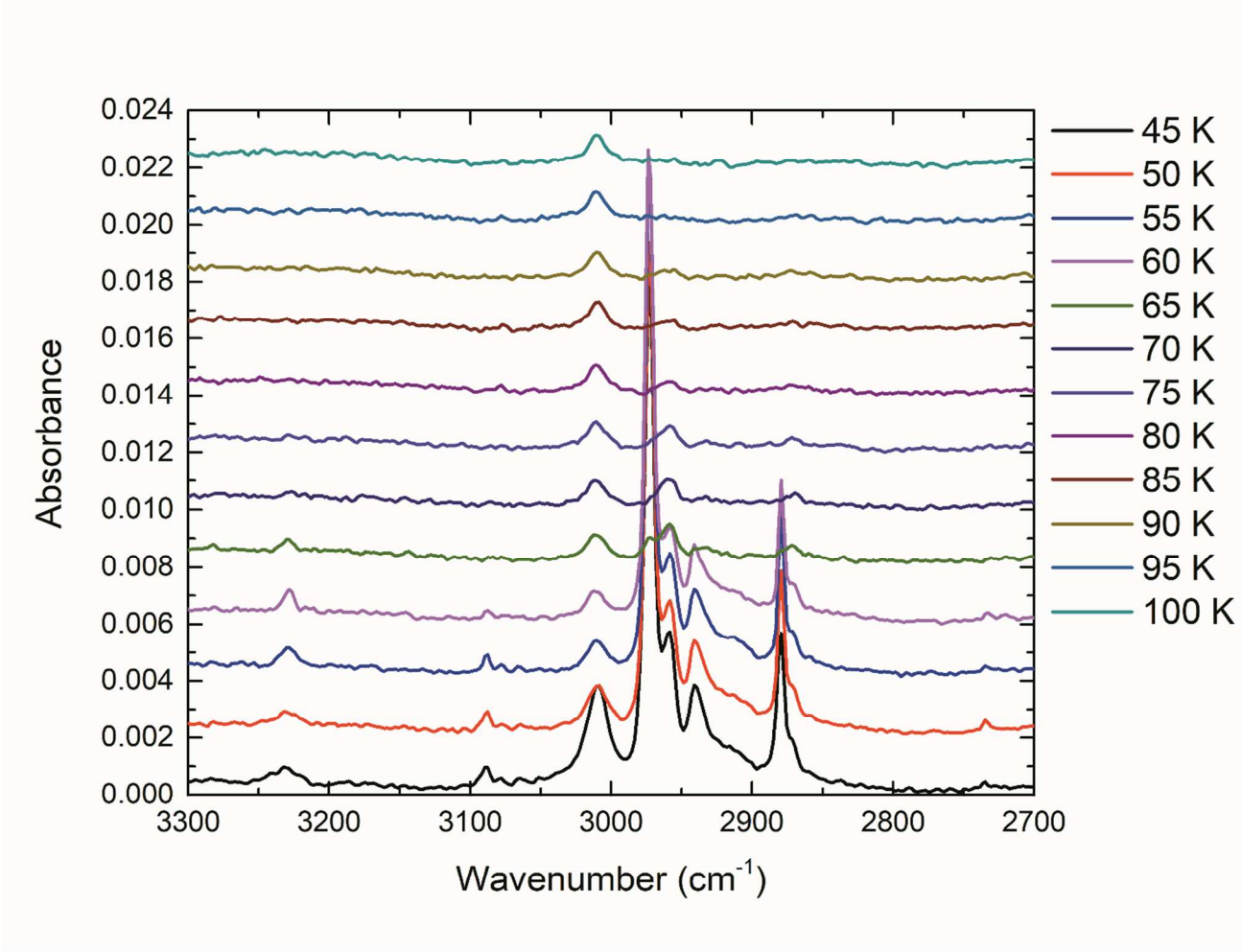

Fig. 4 Infrared spectra from 3300-2700 cm^{-1} after methane ice irradiation during TPD after the majority of the methane reactant has sublimed (see text for peak assignments).

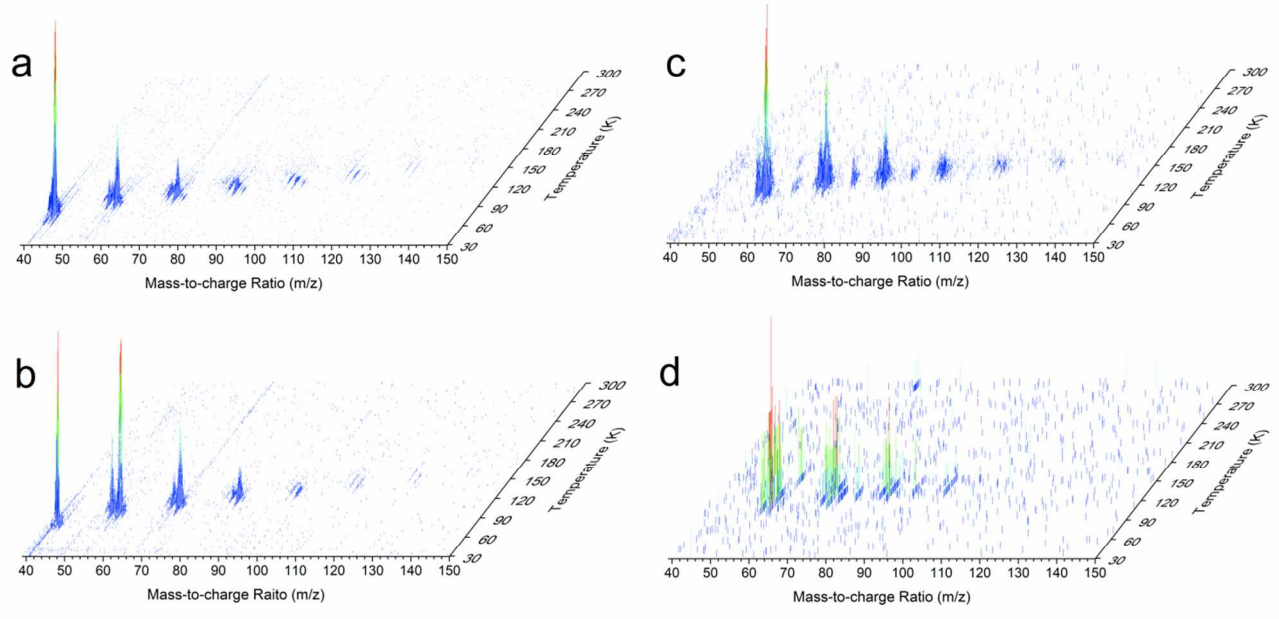

Fig. 5 PI-ReTOF-MS data versus temperature at the PI energies of (a) 10.49 eV, (b) 9.77 eV, (c) 9.45 eV, and (d) 9.15 eV. The signal intensity is color coded where blue corresponds to 1-25 %, cyan to 25-50 %, green to 50-75%, and red to 75-100% of the max intensity detected in each graph.

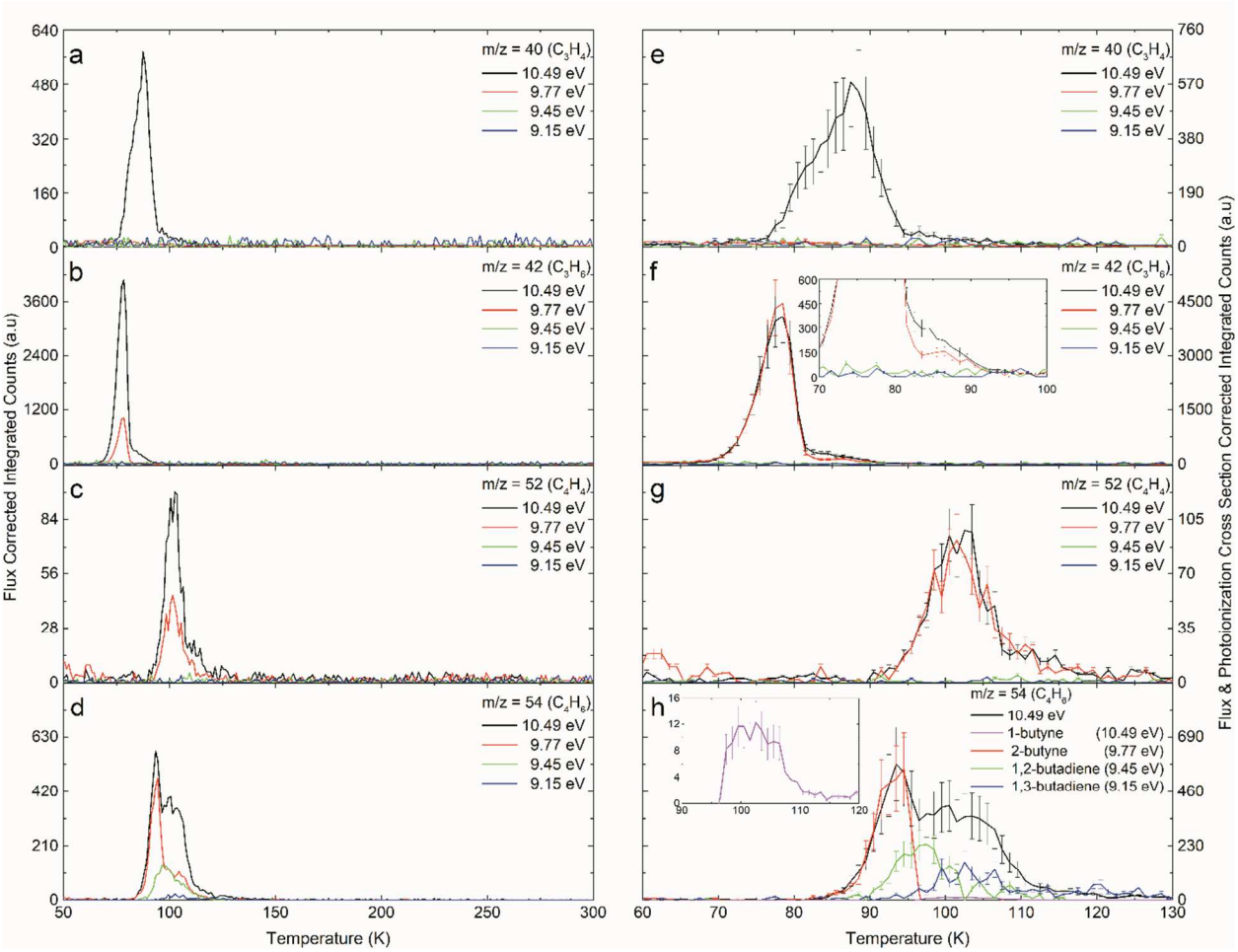

Fig. 6 PI-ReTOF-MS photon flux corrected signals for (a) *m/z* = 40 (C_3H_4), (b) *m/z* = 42 (C_3H_6), (c) *m/z* = 52 (C_4H_4), (d) *m/z* = 54 (C_4H_6), as well as photoionization cross section corrected signals (e) *m/z* = 40 (C_3H_4), (f) *m/z* = 42 (C_3H_6), (g) *m/z* = 52 (C_4H_4), (h) *m/z* = 54 (C_4H_6) at PI energies of 10.49 eV (black), 9.77 eV (red), 9.45 eV (green), and 9.15 eV (blue). Panel h profiles correspond to the noted isomer in the legend determined via subtraction of overlapping isomers (see text). The green (9.45 eV) and blue (9.15 eV) traces have been magnified by a factor of 10 in panels a and e, and a factor of 20 in panels b and f to be visible.

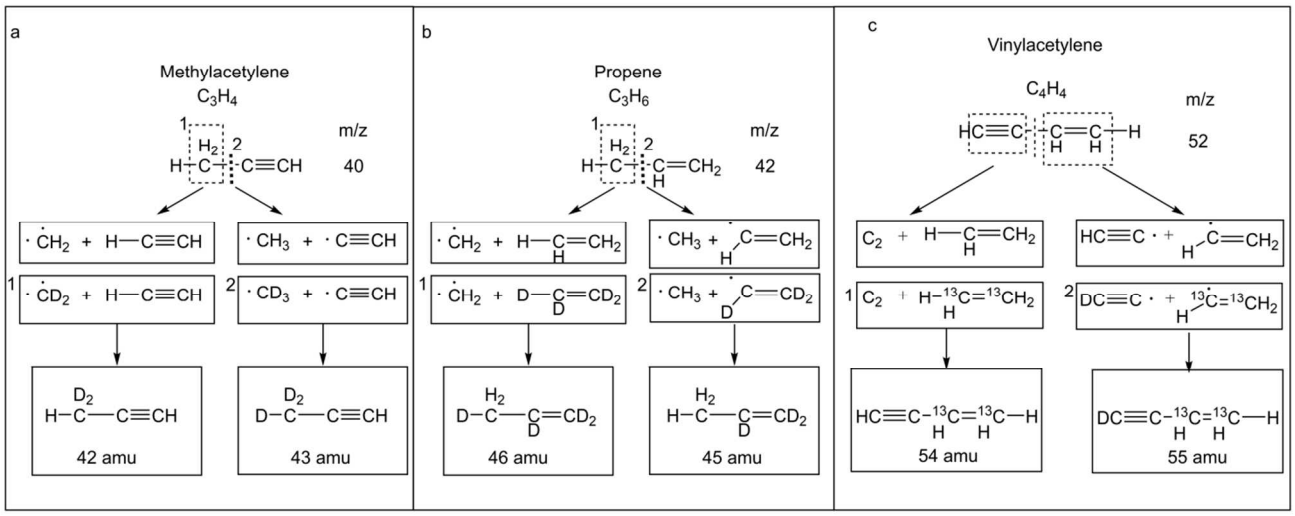

Fig. 7 Mechanisms from isotopic substitution for (a) methylacetylene, (b) propene, and (c) vinylacetylene.

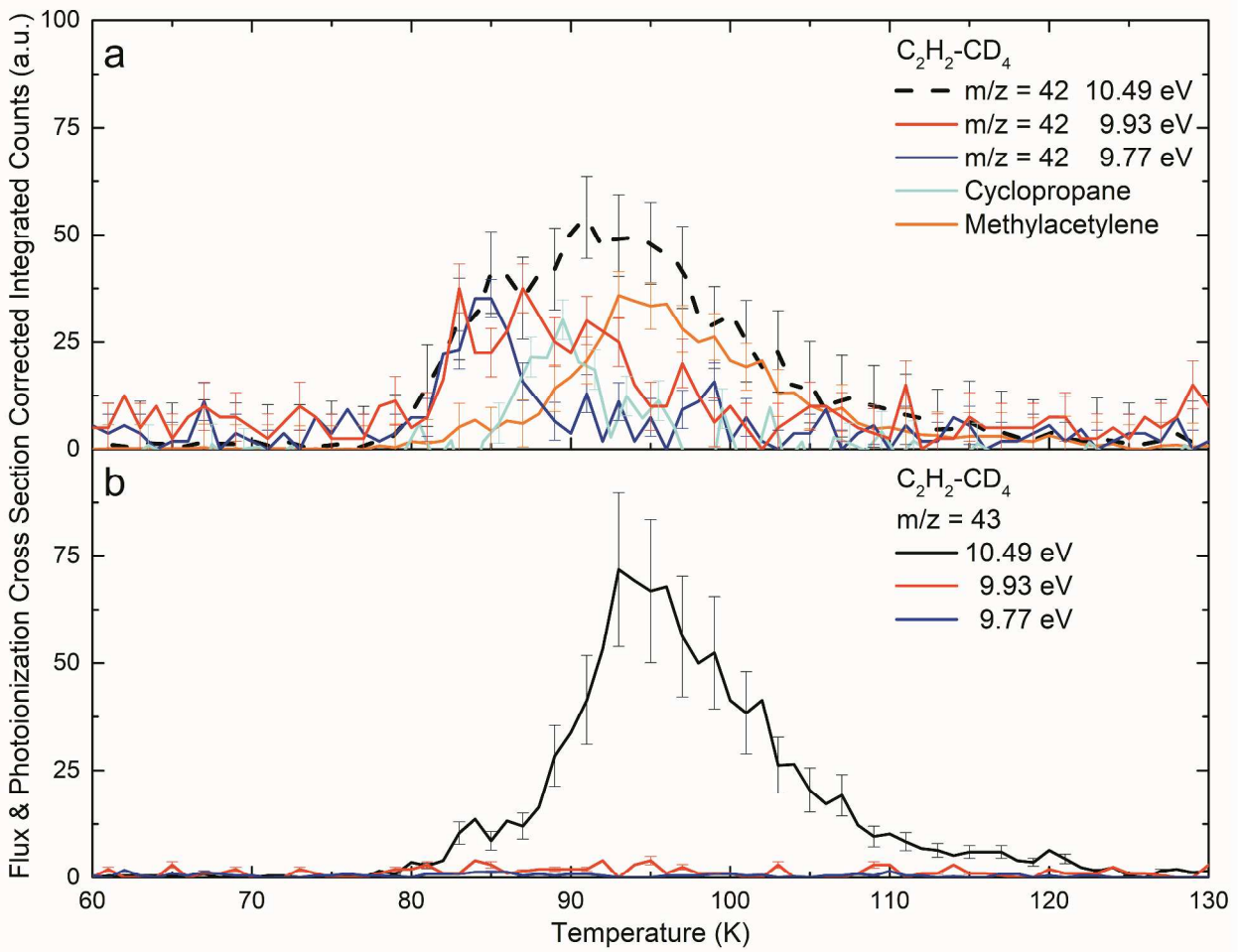

Fig. 8 PI-ReTOF-MS flux and photoionization cross section corrected signals using photoionization energies of 10.49 eV (black), 9.93 eV (red), and 9.77 eV (blue) for (a) *m/z* = 42 which was determined to be due to methylacetylene (orange), cyclopropane (cyan), and most likely propene (blue) and (b) *m/z* = 43 from the irradiated C_2H_2-CD_4 ice mixture (see text for details).

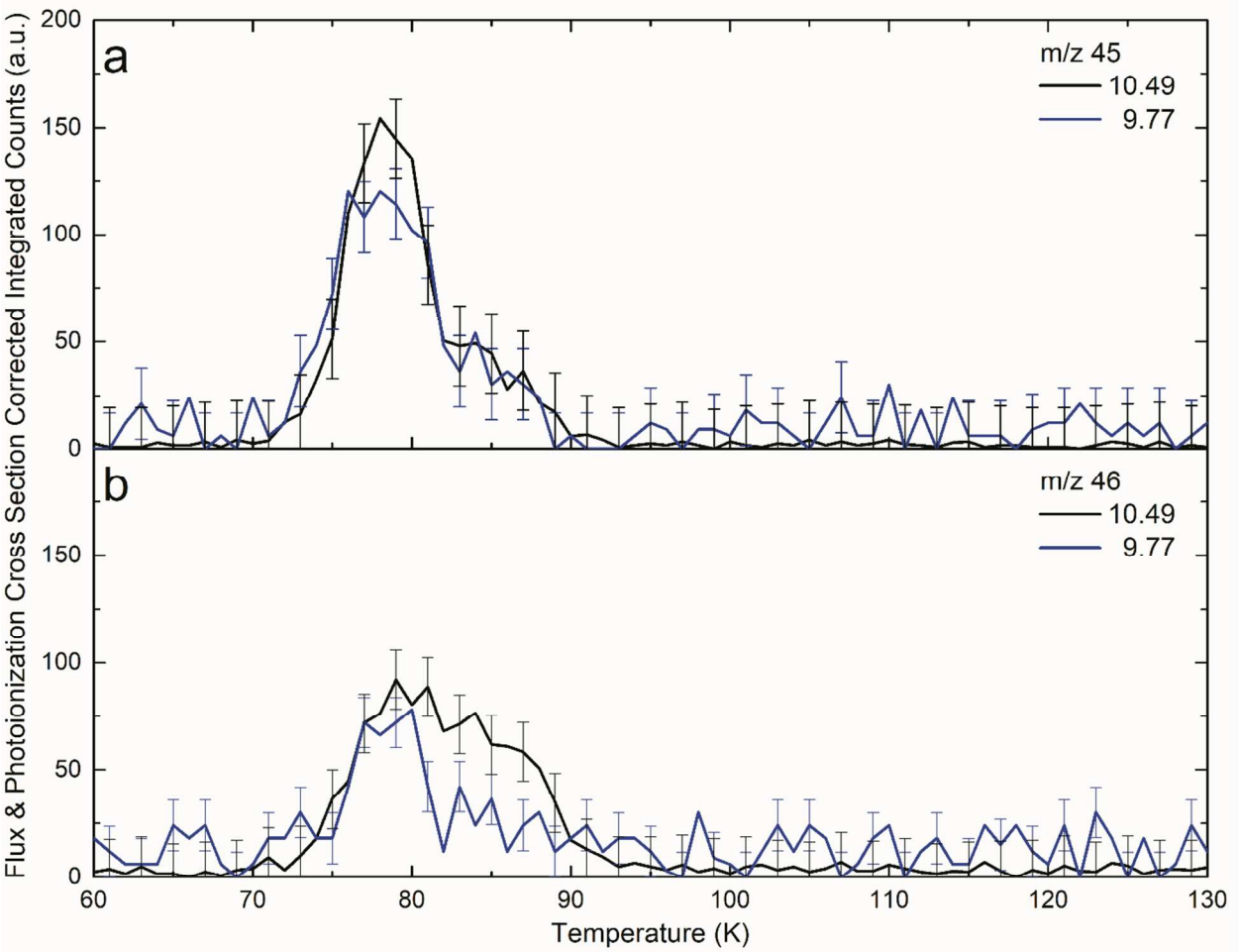

Fig. 9 PI-ReTOF-MS flux and photoionization cross section corrected signals for (a) *m/z* = 45 and (b) *m/z* = 46 using photoionization energies of 10.49 eV (black) and 9.77 eV (blue), from the irradiated C_2D_4-CH_4 ice mixture

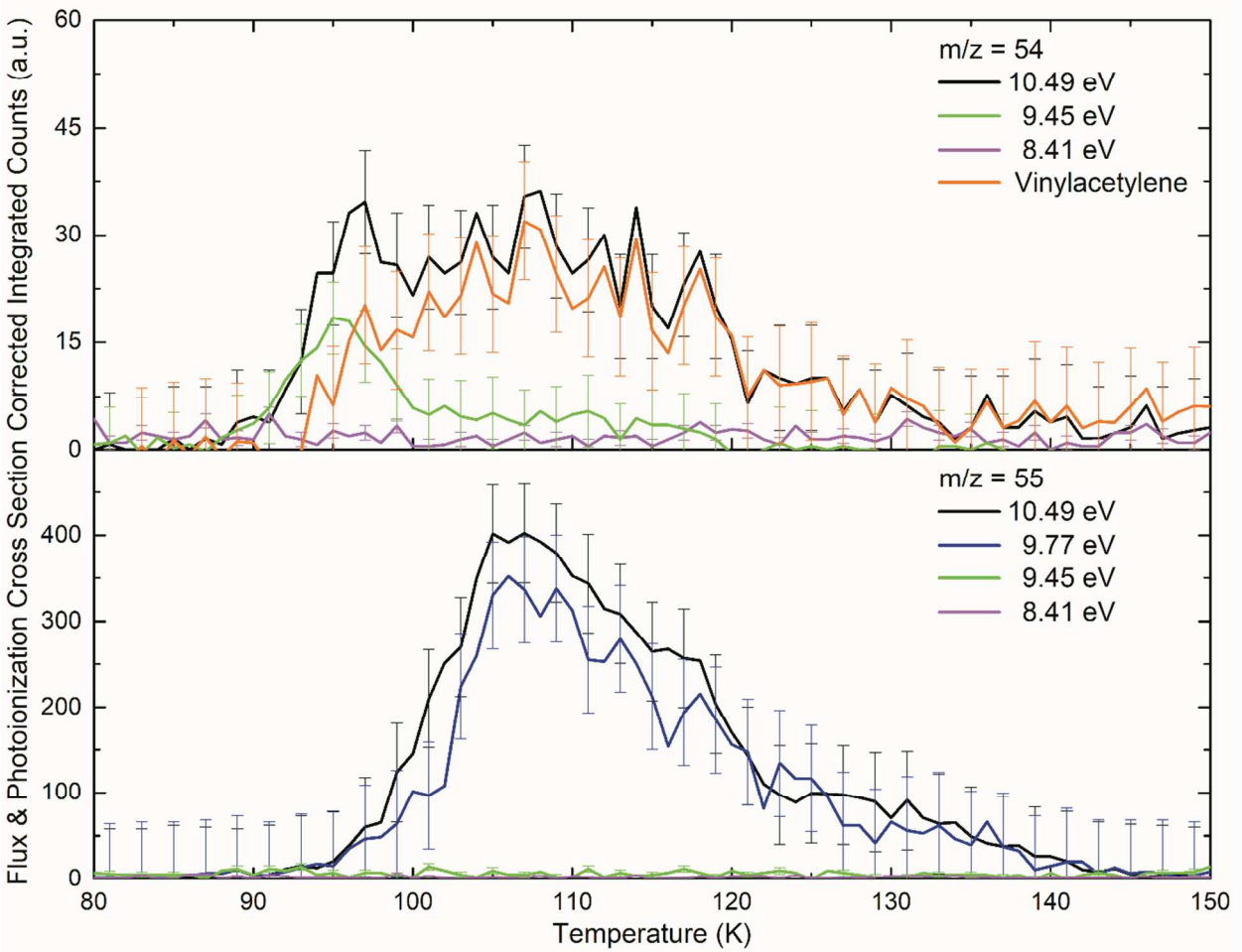

Fig. 10 PI-ReTOF-MS flux and photoionization cross section corrected signals utilizing photoionization energies of 10.49 eV (black), 9.77 eV (blue), 9.45 eV (green), and 8.41 eV (pink) for (a) *m/z* = 54 which was determined to be due to vinylacetylene (orange) and 1,2,3-butatriene (green) and (b) *m/z* = 55, which was due only to vinylacetylene, from the irradiated $^{13}C_2H_4$-C_2D_2 ice mixture

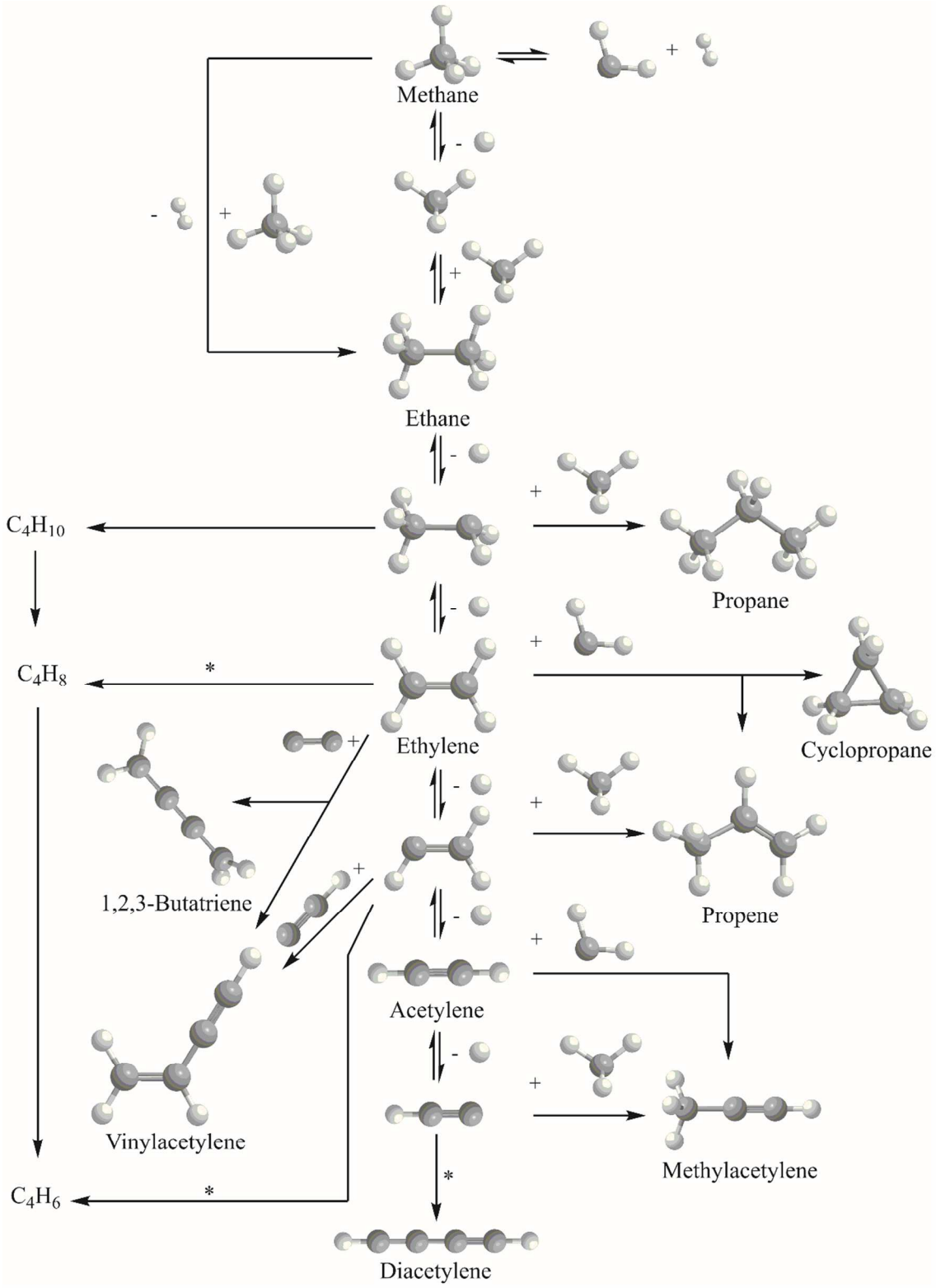

Fig. 11 The experimentally determined dominating reaction pathways for the formation of C2 hydrocarbons, as well as C_3H_4, C_3H_6, and C_4H_4 isomers from methane ices (* designates reaction pathways to be elucidated).

Table 1 **Yields of detected C_3H_4, C_3H_6, C_4H_4, and C_4H_6 isomers**		
Molecule	**Molecules eV^{-1}**	**Relative Ratio**
C_3H_4		
Methylacetylene	**$2.17 \pm 0.95 \times 10^{-4}$**	**-**
C_3H_6		
Propene	**$3.7 \pm 1.5 \times 10^{-3}$**	**$30 \pm 22 : 1 \pm 0.75$ (propene : cyclopropane)**
Cyclopropane	**$1.23 \pm 0.77 \times 10^{-4}$**	
C_4H_4		
Vinylacetylene	**$1.90 \pm 0.84 \times 10^{-5}$**	**-**
C_4H_6		
1,3-butadiene	**$1.41 \pm 0.72 \times 10^{-4}$**	**$3.5 \pm 2.5 : 4.9 \pm 3.4 : 1 \pm 0.7 : 3.2 \pm 2.3$ (1,3-butadiene : 1,2-butadiene : 2-butyne : 1-butyne)**
1,2-butadiene	**$1.97 \pm 0.98 \times 10^{-4}$**	
2-butyne	**$4.01 \pm 1.98 \times 10^{-5}$**	
1-butyne	**$1.28 \pm 0.65 \times 10^{-4}$**	

Table 2 **Reaction pathways and energetics for methylacetylene, propene, and vinylacetylene**

Reaction	Reaction	Reaction Energy ($\Delta_R G$)[a]		Reaction Barrier (E_b)	
		kJ mol^{-1}	eV	kJ mol^{-1}	eV
1	$CH_4\ (X^1A_1) \rightarrow CH_3\ (X^2A_2'') + H\ (^2S_{1/2})$	429	4.44	-	-
2	$CH_4\ (X^1A_1) \rightarrow CH_2\ (a^1A_1) + H_2\ (X^1\Sigma_g^+)$	495	5.13	-	-
3	$C_2H_2\ (X^1\Sigma_g^+) \rightarrow C_2H\ (X^2\Sigma^+) + H\ (^2S_{1/2})$	553	5.73	-	-
4	$CH_3\ (X^2A_2'') + C_2H\ (X^2\Sigma^+) \rightarrow CH_3CCH\ (X^1A')$	-523	-5.42	-	-
5	$CH_2\ (a^1A_1) + C_2H_2\ (X^1\Sigma_g^+) \rightarrow CH_3CCH\ (X^1A')$	-465	-4.82	-	-
6	$CH_3\ (X^2A_2'') + C_2H_2\ (X^1\Sigma_g^+) \rightarrow CH_3CCH\ (X^1A') + H\ (^2S_{1/2})$	30	0.31	33[b]	0.34[b]
7	$C_2H_4\ (X^1A_g) \rightarrow C_2H_3\ (X^2A') + H\ (^2S_{1/2})$	454	4.71	-	-
8	$CH_2\ (a^1A_1) + C_2H_4\ (X^1A_g) \rightarrow CH_3CHCH_2\ (X^1A')$	-455	-4.72	-	-
9	$CH_3\ (X^2A_2'') + C_2H_3\ (X^2A') \rightarrow CH_3CHCH_2\ (X^1A')$	-414	-4.29	-	-
10	$CH_3\ (X^2A_2'') + C_2H_4\ (X^1A_g) \rightarrow CH_3CHCH_2\ (X^1A') + H\ (^2S_{1/2})$	40	0.41	185[b]	1.92[b]
11	$C_2H\ (X^2\Sigma^+) \rightarrow C_2\ (X^1\Sigma_g^+) + H\ (^2S_{1/2})$	473	4.90	-	-
12	$C_2\ (X^1\Sigma_g^+) + C_2H_4\ (X^1A_g) \rightarrow CH_2CHCCH\ (X^1A')$	-588	-6.09	-	-
13	$C_2H\ (X^2\Sigma^+) + C_2H_3\ (X^2A') \rightarrow CH_2CHCCH\ (X^1A')$	-569	-5.90	-	-
14	$C_2H_2\ (X^1\Sigma_g^+) + C_2H_3\ (X^2A') \rightarrow CH_2CHCCH\ (X^1A') + H\ (^2S_{1/2})$	-16	-0.17	6.2[c]	0.06[c]
15	$C_2H\ (X^2\Sigma^+) + C_2H_4\ (X^1A_g) \rightarrow CH_2CHCCH\ (X^1A') + H\ (^2S_{1/2})$	-115	-1.19	-[c]	-[c]

References & Notes:[a]Reaction energies using NIST Chemistry WebBook (https://webbook.nist.gov/chemistry/); [b]Ryazantsev et al. (2015); [c]Krishtal et al. (2009)

REFERENCES AND NOTES

1. A. M. Mebel, A. Landera and R. I. Kaiser, *J. Phys. Chem. A*, 2017, 121, 901-926.
2. E. Herbst, *Int. Rev. Phys. Chem.*, 2017, 36, 287-331.
3. D. S. N. Parker and R. I. Kaiser, *Chem. Soc. Rev.*, 2017, 46, 452-463.
4. D. S. N. Parker, R. I. Kaiser, O. Kostko and M. Ahmed, *ChemPhysChem*, 2015, 16, 2091-2093.
5. D. S. N. Parker, F. Zhang, R. I. Kaiser, V. V. Kislov and A. M. Mebel, *Chemistry–An Asian Journal*, 2011, 6, 3035-3047.
6. F. Zhang, R. I. Kaiser, V. V. Kislov, A. M. Mebel, A. Golan and M. Ahmed, *J. Phys. Chem. Lett.*, 2011, 2, 1731-1735.
7. T. Yang, D. S. N. Parker, B. B. Dangi, R. I. Kaiser and A. M. Mebel, *Phys. Chem. Chem. Phys.*, 2015, 17, 10510-10519.
8. F. Zhang, S. Kim and R. I. Kaiser, *Phys. Chem. Chem. Phys.*, 2009, 11, 4707 - 4714.
9. F. Goulay, D. L. Osborn, C. A. Taatjes, P. Zou, G. Meloni and S. R. Leone, *Phys. Chem. Chem. Phys.*, 2007, 9, 4291-4300.
10. A. B. Vakhtin, D. E. Heard, I. W. M. Smith and S. R. Leone, *Chem. Phys. Lett.*, 2001, 344, 317-324.
11. F. Zhang, Y. S. Kim, R. I. Kaiser, S. P. Krishtal and A. M. Mebel, *J. Phys. Chem. A*, 2009, 113, 11167-11173.
12. R. I. Kaiser, D. Stranges, H. M. Bevsek, Y. T. Lee and A. G. Suits, *J. Chem. Phys.*, 1997, 106, 4945-4953.
13. B. B. Dangi, S. Maity, R. I. Kaiser and A. M. Mebel, *J. Phys. Chem. A*, 2013, 117, 11783-11793.
14. A. M. Mebel and R. I. Kaiser, *Int. Rev. Phys. Chem.*, 2015, 34, 461-514.
15. Y. S. Kim and R. I. Kaiser, *Astrophys. J., Suppl. Ser.*, 2009, 181, 543.
16. V. Vuitton, R. V. Yelle, P. Lavvas and S. J. Klippenstein, *Astrophys. J.*, 2012, 744, 11.
17. F. Zhang, D. Parker, S. Kim, R. I. Kaiser and A. M. Mebel, *Astrophys. J.*, 2011, 728, 141.
18. D. S. N. Parker, F. Zhang, Y. S. Kim, R. I. Kaiser, A. Landera, V. V. Kislov, A. M. Mebel and A. G. G. M. Tielens, *Proc. Natl. Acad. Sci. U. S. A.*, 2012, 109, 53-58.
19. D. S. N. Parker, B. B. Dangi, R. I. Kaiser, A. Jamal, M. N. Ryazantsev, K. Morokuma, A. Korte and W. Sander, *J. Phys. Chem. A*, 2014, 118, 2709-2718.
20. T. Yang, L. Muzangwa, R. I. Kaiser, A. Jamal and K. Morokuma, *Phys. Chem. Chem. Phys.*, 2015, 17, 21564-21575.
21. F. Zhang, B. Jones, P. Maksyutenko, R. I. Kaiser, C. Chin, V. V. Kislov and A. M. Mebel, *J. Am. Chem. Soc.*, 2010, 132, 2672-2683.
22. D. S. N. Parker, B. B. Dangi, R. I. Kaiser, A. Jamal, M. Ryazantsev and K. Morokuma, *J. Phys. Chem. A*, 2014, 118, 12111-12119.
23. B. M. Jones, F. Zhang, R. I. Kaiser, A. Jamal, A. M. Mebel, M. A. Cordiner and S. B. Charnley, *Proc. Natl. Acad. Sci. U. S. A.*, 2011, 108, 452-457.
24. L. E. Snyder and D. Buhl, *Nature Physical Science*, 1973, 243, 45.
25. F. J. Lovas, D. R. Johnson, D. Buhl and L. E. Snyder, *Astrophys. J.*, 1976, 209, 770-777.
26. W. Irvine, B. Hoglund, P. Friberg, J. Askne and J. Ellder, *Astrophys. J.*, 1981, 248, L113-L117.
27. K. M. Hickson, V. Wakelam and J.-C. Loison, *Molecular Astrophysics*, 2016, 3-4, 1-9.
28. V. V. Guzmán, J. Pety, P. Gratier, J. R. Goicoechea, M. Gerin, E. Roueff, F. Le Petit and J. Le Bourlot, *Faraday Discuss.*, 2014, 168, 103.
29. C. Vastel, C. Ceccarelli, B. Lefloch and R. Bachiller, *Astrophys. J., Lett.*, 2014, 795, L2.
30. F. Costagliola, K. Sakamoto, S. Muller, S. Martín, S. Aalto, N. Harada, P. van der Werf, S. Viti, S. Garcia-Burillo and M. Spaans, *Astron. Astrophys.*, 2015, 582, A91.

31. S. Muller, F. Combes, M. Guélin, M. Gérin, S. Aalto, A. Beelen, J. H. Black, S. J. Curran, J. Darling, D. V-Trung, S. García-Burillo, C. Henkel, C. Horellou, S. Martín, I. Martí-Vidal, K. M. Menten, M. T. Murphy, J. Ott, T. Wiklind and M. A. Zwaan, *Astron. Astrophys.*, 2014, 566, A112.
32. A. Belloche, H. S. Müller, K. M. Menten, P. Schilke and C. Comito, *Astron. Astrophys.*, 2013, 559, 1-187.
33. K. I. Öberg, M. D. Boamah, E. C. Fayolle, R. T. Garrod, C. J. Cyganowski and F. v. d. Tak, *Astrophys. J.*, 2013, 771, 95.
34. N. Marcelino, J. Cernicharo, M. Agúndez, E. Roueff, M. Gerin, J. Martín-Pintado, R. Mauersberger and C. Thum, *Astrophys. J.*, 2007, 665, L127.
35. T. Fouchet, B. Bezard, E. Lellouch, H. Feuchtgruber, P. Drossart and T. Encrenaz, *Astron. Astrophys.*, 2000, 355, L13-L17.
36. T. de Graauw, H. Feuchtgruber, B. Bézard, P. Drossart, T. Encrenaz, D. Beintema, M. Griffin, A. Heras, M. Kessler and K. Leech, *Astron. Astrophys*, 1997, 321, L13-L16.
37. M. Burgdorf, G. Orton, J. van Cleve, V. Meadows and J. Houck, *Icarus*, 2006, 184, 634-637.
38. N. A. Teanby, P. G. J. Irwin, R. de Kok, A. Jolly, B. Bézard, C. A. Nixon and S. B. Calcutt, *Icarus*, 2009, 202, 620-631.
39. M. Agúndez, J. Cernicharo and M. Guélin, *Astron. Astrophys.*, 2015, 577, L5.
40. C. A. Nixon, D. E. Jennings, B. Bézard, S. Vinatier, N. A. Teanby, K. Sung, T. M. Ansty, P. G. J. Irwin, N. Gorius, V. Cottini, A. Coustenis and F. M. Flasar, *Astrophys. J., Lett.*, 2013, 776, L14.
41. R. I. Kaiser, D. S. N. Parker, F. Zhang, A. Landera, V. V. Kislov and A. M. Mebel, *J. Phys. Chem. A*, 2012, 116, 4248-4258.
42. L. G. Muzangwa, T. Yang, D. S. N. Parker, R. I. Kaiser, A. M. Mebel, A. Jamal, M. Ryazantsev and K. Morokuma, *Phys. Chem. Chem. Phys.*, 2015, 17, 7699-7706.
43. R. Le Gal, E. Herbst, G. Dufour, P. Gratier, M. Ruaud, T. H. G. Vidal and V. Wakelam, *Astron. Astrophys.*, 2017, 605, A88.
44. Z. Lin, D. Talbi, E. Roueff, E. Herbst, N. Wehres, C. A. Cole, Z. Yang, T. P. Snow and V. M. Bierbaum, *Astrophys. J.*, 2013, 765, 80.
45. J. M. C. Rawlings, D. A. Williams, S. Viti and C. Cecchi-Pestellini, *Mon. Not. R. Astron. Soc.*, 2013, 436, L59-L63.
46. J. M. C. Rawlings, D. A. Williams, S. Viti, C. Cecchi-Pestellini and W. W. Duley, *Mon. Not. R. Astron. Soc.* , 2013, 430, 264-273.
47. J. M. C. Rawlings, D. A. Williams, S. Viti, C. Cecchi-Pestellini and W. W. Duley, *Faraday Discuss.*, 2014, 168, 369-388.
48. J. Bouwman, F. Goulay, S. R. Leone and K. R. Wilson, *J. Phys. Chem. A*, 2012, 116, 3907-3917.
49. D. S. N. Parker, A. M. Mebel and R. I. Kaiser, *Chem. Soc. Rev.*, 2014, 43, 2701-2713.
50. J.-C. Loison and A. Bergeat, *Phys. Chem. Chem. Phys.*, 2009, 11, 655-664.
51. D. E. Woon and J.-Y. Park, *Icarus*, 2009, 202, 642-655.
52. S. P. Krishtal, A. M. Mebel and R. I. Kaiser, *J. Phys. Chem. A*, 2009, 113, 11112-11128.
53. L. Zhou, W. Zheng, R. I. Kaiser, A. Landera, A. M. Mebel, M. C. Liang and Y. L. Yung, *Astrophys. J.*, 2010, 718, 1243.
54. S. H. Cuylle, D. Zhao, G. Strazzulla and H. Linnartz, *Astron. Astrophys.*, 2014, 570, A83.
55. J. Kalvāns and I. Shmeld, *Astron. Astrophys.*, 2010, 521, A37.
56. M. P. Redman, S. Viti, P. Cau and D. A. Williams, *MNRAS*, 2003, 345, 1291-1296.
57. D. P. Ruffle and E. Herbst, *Mon. Not. R. Astron. Soc.*, 2001, 322, 770-778.
58. J. M. Ribeiro and A. M. Mebel, *J. Phys. Chem. A*, 2016, 120, 1800-1812.
59. A. J. Trevitt, M. B. Prendergast, F. Goulay, J. D. Savee, D. L. Osborn, C. A. Taatjes and S. R. Leone, *J. Phys. Chem. A*, 2013, 117, 6450-6457.

60. R. I. Kaiser and K. Roessler, *Astrophys. J.*, 1997, 475, 144-154.
61. R. I. Kaiser, G. Eich, A. Gabrysch and K. Roessler, *Astrophys. J.*, 1997, 484, 487-498.
62. W. Zheng, D. Jewitt and R. I. Kaiser, *Astrophys. J.*, 2006, 648, 753.
63. B. M. Jones, C. J. Bennett and R. I. Kaiser, *Astrophys. J.*, 2011, 734, 78-90.
64. A. C. A. Boogert, P. A. Gerakines and D. C. B. Whittet, *Annu. Rev. Astron. Astrophys.*, 2015, 53, 541-581.
65. W. M. Grundy, R. P. Binzel, B. J. Buratti, J. C. Cook, D. P. Cruikshank, C. M. Dalle Ore, A. M. Earle, K. Ennico, C. J. A. Howett, A. W. Lunsford, C. B. Olkin, A. H. Parker, S. Philippe, S. Protopapa, E. Quirico, D. C. Reuter, B. Schmitt, K. N. Singer, A. J. Verbiscer, R. A. Beyer, M. W. Buie, A. F. Cheng, D. E. Jennings, I. R. Linscott, J. W. Parker, P. M. Schenk, J. R. Spencer, J. A. Stansberry, S. A. Stern, H. B. Throop, C. C. C. Tsang, H. A. Weaver, G. E. Weigle and L. A. Young, *Science*, 2016, 351.
66. M. W. Telfer, E. J. R. Parteli, J. Radebaugh, R. A. Beyer, T. Bertrand, F. Forget, F. Nimmo, W. M. Grundy, J. M. Moore, S. A. Stern, J. Spencer, T. R. Lauer, A. M. Earle, R. P. Binzel, H. A. Weaver, C. B. Olkin, L. A. Young, K. Ennico and K. Runyon, *Science*, 2018, 360, 992.
67. B. M. Jones and R. I. Kaiser, *J. Phys. Chem. Lett.*, 2013, 4, 1965-1971.
68. R. I. Kaiser, S. Maity and B. M. Jones, *Phys. Chem. Chem. Phys.*, 2014, 16, 3399-3424.
69. R. I. Kaiser, S. Maity and B. M. Jones, *Angew. Chem., Int. Ed.*, 2015, 54, 195-200.
70. S. Maity, R. I. Kaiser and B. M. Jones, *Astrophys. J.*, 2014, 789, 36.
71. S. Maity, R. I. Kaiser and B. M. Jones, *Faraday Discuss.*, 2014, 168, 485.
72. S. Maity, R. I. Kaiser and B. M. Jones, *Phys. Chem. Chem. Phys.*, 2015, 17, 3081-3114.
73. M. Förstel, P. Maksyutenko, B. M. Jones, B.-J. Sun, S.-H. Chen, A. H. H. Chang and R. I. Kaiser, *ChemPhysChem*, 2015, 16, 3139-3142.
74. M. Förstel, P. Maksyutenko, B. M. Jones, B. J. Sun, H. C. Lee, A. H. H. Chang and R. I. Kaiser, *Astrophys. J.*, 2016, 820, 117.
75. M. Förstel, Y. A. Tsegaw, P. Maksyutenko, A. M. Mebel, W. Sander and R. I. Kaiser, *ChemPhysChem*, 2016, 17, 2726-2735.
76. M. Förstel, P. Maksyutenko, B. M. Jones, B. J. Sun, A. H. H. Chang and R. I. Kaiser, *Chem. Commun. (Cambridge, U. K.)*, 2016, 52, 741-744.
77. G. Tarczay, M. Förstel, P. Maksyutenko and R. I. Kaiser, *Inorg. Chem.*, 2016, 55, 8776-8785.
78. M. J. Abplanalp, A. Borsuk, B. M. Jones and R. I. Kaiser, *Astrophys. J.*, 2015, 814, 45-61.
79. M. J. Abplanalp, S. Gozem, A. I. Krylov, C. N. Shingledecker, E. Herbst and R. I. Kaiser, *Proc. Natl. Acad. Sci. U. S. A.*, 2016, 113, 7727-7732.
80. M. J. Abplanalp, M. Förstel and R. I. Kaiser, *Chem. Phys. Lett.*, 2016, 644, 79-98.
81. P. Maksyutenko, L. G. Muzangwa, B. M. Jones and R. I. Kaiser, *Phys. Chem. Chem. Phys.*, 2015, 17, 7514-7527.
82. P. Maksyutenko, M. Förstel, P. Crandall, B.-J. Sun, M.-H. Wu, A. H. H. Chang and R. I. Kaiser, *Chem. Phys. Lett.*, 2016, 658, 20-29.
83. A. Bergantini, R. Frigge and R. I. Kaiser, *Astrophys. J.*, 2018, 859, 59.
84. S. Góbi, M. Förstel, P. Maksyutenko and R. I. Kaiser, *Astrophys. J.*, 2017, 835, 241.
85. C. Zhu, R. Frigge, A. M. Turner, R. I. Kaiser, B.-J. Sun, S.-Y. Chen and A. H. H. Chang, *Chem. Commun.*, 2018, 54, 5716-5719.
86. A. Bergantini, S. Góbi, M. J. Abplanalp and R. I. Kaiser, *Astrophys. J.*, 2018, 852, 70.
87. P. Groner, I. Stolkin and H. H. Gunthard, *J. Phys. E: Sci. Instrum.*, 1973, 6, 122.
88. B. M. Jones, R. I. Kaiser and G. Strazzulla, *Astrophys. J.*, 2014, 781, 85.
89. B. M. Jones, R. I. Kaiser and G. Strazzulla, *Astrophys. J.*, 2014, 788, 170.
90. P. A. Gerakines and R. L. Hudson, *Astrophys. J., Lett.*, 2015, 805, L20.
91. S. Góbi, A. Bergantini and R. I. Kaiser, *Astrophys. J.*, 2017, 838, 84.

92. S. Góbi, A. Bergantini, A. M. Turner and R. I. Kaiser, *J. Phys. Chem. A*, 2017, 121, 3879-3890.
93. Y. A. Tsegaw, S. Góbi, M. Förstel, P. Maksyutenko, W. Sander and R. I. Kaiser, *J. Phys. Chem. A*, 2017, 121, 7477-7493.
94. S. Góbi, P. B. Crandall, P. Maksyutenko, M. Förstel and R. I. Kaiser, *J. Phys. Chem. A*, 2018, 122, 2329-2343.
95. R. I. Kaiser and P. Maksyutenko, *J. Phys. Chem. C*, 2015, 119, 14653-14668.
96. G. Tarczay, M. Förstel, S. Góbi, P. Maksyutenko and R. I. Kaiser, *ChemPhysChem*, 2017, 18, 882-889.
97. D. Drouin, A. R. Couture, D. Joly, X. Tastet, V. Aimez and R. Gauvin, *Scanning*, 2007, 29, 92-101.
98. M. Á. Satorre, M. Domingo, C. Millán, R. Luna, R. Vilaplana and C. Santonja, *Planet. Space Sci.*, 2008, 56, 1748-1752.
99. A. I. Prokhvatilov and A. P. Isakina, *Phys. Status Solidi A*, 1983, 78, 147-155.
100. M. J. Abplanalp, B. M. Jones and R. I. Kaiser, *Phys. Chem. Chem. Phys.*, 2018, 20, 5435-5468.
101. M. H. Moore and R. L. Hudson, *Proc. Int. Astron. Union*, 2006, 1, 247.
102. A. M. Turner, M. J. Abplanalp, S. Y. Chen, Y. T. Chen, A. H. H. Chang and R. I. Kaiser, *Phys. Chem. Chem. Phys.*, 2015, 17, 27281-27291.
103. M. Förstel, P. Maksyutenko, A. M. Mebel and R. I. Kaiser, *Astrophys. J., Lett.*, 2016, 818, L30.
104. S. Góbi, A. Bergantini and R. I. Kaiser, *Astrophys. J.*, 2016, 832, 164.
105. A. Bergantini, P. Maksyutenko and R. I. Kaiser, *Astrophys. J.*, 2017, 841, 96.
106. M. Förstel, A. Bergantini, P. Maksyutenko, S. Góbi and R. I. Kaiser, *Astrophys. J.*, 2017, 845, 83.
107. M. J. Abplanalp, S. Góbi, A. Bergantini, A. M. Turner and R. I. Kaiser, *ChemPhysChem*, 2018, 19, 556-560.
108. M. J. Abplanalp and R. I. Kaiser, *Astrophys. J.*, 2016, 827, 132.
109. M. J. Abplanalp and R. I. Kaiser, *Astrophys. J.*, 2017, 836, 195.
110. NIST Standard Reference Database Number 69, http://webbook.nist.gov/chemistry/ie-ser/, (August 21, 2017)
111. R. I. Kaiser and P. Maksyutenko, *Chem. Phys. Lett.*, 2015, 631–632, 59-65.
112. A. M. Turner, M. J. Abplanalp and R. I. Kaiser, *Astrophys. J.*, 2016, 819, 97.
113. M. N. Ryazantsev, A. Jamal, S. Maeda and K. Morokuma, *Phys. Chem. Chem. Phys.*, 2015, 17, 27789-27805.
114. R. Gómez-Balderas, M. L. Coote, D. J. Henry and L. Radom, *J. Phys. Chem. A*, 2004, 108, 2874-2883.
115. A. M. Mebel, V. V. Kislov and R. I. Kaiser, *J. Chem. Phys.*, 2006, 125, 133113.
116. A. M. Mebel, V. V. Kislov and R. I. Kaiser, *J. Am. Chem. Soc.*, 2008, 130, 13618-13629.
117. D. S. N. Parker, T. Yang, R. I. Kaiser, A. Landera and A. M. Mebel, *Chem. Phys. Lett.*, 2014, 595-596, 230-236.
118. D. S. N. Parker, R. I. Kaiser, T. P. Troy and M. Ahmed, *Angew. Chem., Int. Ed.*, 2014, 53, 7740-7744.
119. R. I. Kaiser, D. S. N. Parker and A. M. Mebel, *Annu. Rev. Phys. Chem.*, 2015, 66, 43-67.
120. T. Yang, L. Muzangwa, D. S. N. Parker, R. I. Kaiser and A. M. Mebel, *Phys. Chem. Chem. Phys.*, 2015, 17, 530-540.
121. A. Landera, R. I. Kaiser and A. M. Mebel, *J. Chem. Phys.*, 2011, 134, 024302.
122. F. Zhang, X. Gu and R. I. Kaiser, *J. Chem. Phys.*, 2008, 128, 084315.
123. D. S. N. Parker, R. I. Kaiser, B. Bandyopadhyay, O. Kostko, T. P. Troy and M. Ahmed, *Angew. Chem., Int. Ed.*, 2015, 54, 5421-5424.
124. T. Yang, T. P. Troy, B. Xu, O. Kostko, M. Ahmed, A. M. Mebel and R. I. Kaiser, *Angew. Chem., Int. Ed.*, 2016, 55, 14983-14987.

125. T. Yang, R. I. Kaiser, T. P. Troy, B. Xu, O. Kostko, M. Ahmed, A. M. Mebel, M. V. Zagidullin and V. N. Azyazov, *Angew. Chem., Int. Ed.*, 2017, 56, 4515-4519.
126. L. Zhao, R. I. Kaiser, B. Xu, U. Ablikim, M. Ahmed, D. Joshi, G. Veber, F. R. Fischer and A. M. Mebel, *Nature Astronomy*, 2018, 2, 413-419.
127. D. S. N. Parker, R. I. Kaiser, O. Kostko, T. P. Troy, M. Ahmed, A. M. Mebel and A. G. G. M. Tielens, *Astrophys. J.*, 2015, 803, 53.
128. D. S. N. Parker, T. Yang, B. B. Dangi, R. I. Kaiser, P. P. Bera and T. J. Lee, *Astrophys. J.*, 2015, 815, 115.
129. M. Lu and J. A. Mulholland, *Chemosphere*, 2001, 42, 625-633.
130. H. J. Kimber, C. P. Ennis and S. D. Price, *Faraday Discuss.*, 2014, 168, 167-184.
131. F. Zhang, P. Maksyutenko and R. I. Kaiser, *Phys. Chem. Chem. Phys.*, 2012, 14, 529-537.
132. R. L. Hudson, M. J. Loeffler and K. M. Yocum, *Astrophys. J.*, 2017, 835, 225.
133. B. A. McGuire, P. B. Carroll, R. A. Loomis, I. A. Finneran, P. R. Jewell, A. J. Remijan and G. A. Blake, *Science*, 2016, 352, 1449.
134. A. Bergantini, M. J. Abplanalp, P. Pokhilko, A. I. Krylov, C. N. Shingledecker, E. Herbst and R. I. Kaiser, *Astrophys. J.*, 2018, 862, 140-152.
135. L. Zhao, R. I. Kaiser, B. Xu, U. Ablikim, M. Ahmed, M. V. Zagidullin, V. N. Azyazov, A. H. Howlader, S. F. Wnuk and A. M. Mebel, *J. Phys. Chem. Lett.*, 2018, 9, 2620-2626.
136. A. Golan, M. Ahmed, A. M. Mebel and R. I. Kaiser, *Phys. Chem. Chem. Phys.*, 2013, 15, 341-347.
137. A. M. Thomas, M. Lucas, T. Yang, R. I. Kaiser, L. Fuentes, D. Belisario-Lara and A. M. Mebel, *ChemPhysChem*, 2017, 18, 1971-1976.
138. B. J. Sun, C. H. Huang, S. Y. Chen, S. H. Chen, R. I. Kaiser and A. H. H. Chang, *J. Phys. Chem. A*, 2014, 118, 7715-7724.
139. D. S. N. Parker, S. Maity, B. B. Dangi, R. I. Kaiser, A. Landera and A. M. Mebel, *Phys. Chem. Chem. Phys.*, 2014, 16, 12150-12163.
140. C. J. Bennett, C. S. Jamieson, Y. Osumura and R. I. Kaiser, *Astrophys. J.*, 2006, 653, 792-811.